Downloaded from genome.cshlp.org on November 17, 2026 . Published by Cold Spring Harbor Laboratory Press



# Genomic regulatory landscape underlying the antiviral response of Atlantic salmon

Shahmir Naseer, Thomas Clark, Bertrand Collet, et al.

*Genome Res.* published online October 22, 2025
Access the most recent version at doi:10.1101/gr.280579.125

**P<P** Published online October 22, 2025 in advance of the print journal.

**Open Access** Freely available online through the *Genome Research* Open Access option.

**Creative Commons License** This article, published in *Genome Research*, is available under a Creative Commons License (Attribution-NonCommercial 4.0 International), as described at http://creativecommons.org/licenses/by-nc/4.0/.

**Email Alerting Service** Receive free email alerts when new articles cite this article - sign up in the box at the top right corner of the article or **click here.**




To subscribe to *Genome Research* go to:
**https://genome.cshlp.org/subscriptions**

© 2026 Naseer et al.; Published by Cold Spring Harbor Laboratory Press

Downloaded from genome.cshlp.org on November 17, 2026 . Published by Cold Spring Harbor Laboratory Press



# Genomic regulatory landscape underlying the antiviral response of Atlantic salmon

Shahmir Naseer,[1] Thomas Clark,[1] Bertrand Collet,[2] Pooran Dewari,[3] Damir Baranašić,[4] Daniel J. Macqueen,[3] Pierre Boudinot,[2] and Samuel A.M. Martin[1]

[1] *Scottish Fish Immunology Research Centre, School of Biological Sciences, University of Aberdeen, Aberdeen AB24 2TZ, United Kingdom;* [2] *Université Paris-Saclay, INRAE, UVSQ, VIM, 78350 Jouy-en-Josas, France;* [3] *The Roslin Institute and Royal (Dick) School of Veterinary Studies, University of Edinburgh, Easter Bush Campus, Midlothian EH25 9RG, United Kingdom;* [4] *Ruđer Bošković Institute, Laboratory for Computational Biology and Translational Medicine, Bijenička, 10000 Zagreb, Croatia*

**All jawed vertebrates have a highly coordinated innate immune response to viral infections driven by a core set of interferon-responsive genes (ISGs), but interspecies variation remains substantial. In this study, we examine the genome-wide regulatory basis for antiviral gene expression responses in Atlantic salmon (*Salmo salar*), representing a teleost family that underwent a whole-genome duplication (WGD) event ~100 Mya. We stimulate fish systemically with polyinosinic:polycytidylic acid (poly I:C), a synthetic viral mimic, and profile transcriptomic and epigenomic responses in the primary hematopoietic and lymphoid tissue. We use ATAC-seq and ChIP-seq (H3K27ac and H3K27me3), combined with mRNA-seq, to comprehensively examine modifications in gene regulation following stimulation. We identify a set of 197 ISGs with regulatory elements showing increased chromatin accessibility and H3K27ac signal in concert with increased gene expression in response to poly I:C. Fifty-four of these genes were conserved ISGs in rainbow trout, zebrafish, and humans. Our analysis provides evidence for conserved transcription factors (TFs) driving the interferon response by binding ISG promoters, including IRF8, IRF9, STAT1, and STAT2. Regulatory elements within differentially expressed genes are enriched for predicted binding sites for STAT6, PRDM1, IRF6, JDP2, NR2E1, and BCL6, suggesting a central role for these TFs in the antiviral response. Finally, we demonstrate paralog-specific enrichment of interferon-stimulated response element (ISRE) motifs in poly I:C–activated promoters of ISGs retained as duplicates from the salmonid WGD. Overall, this study provides novel insights into the genomic regulatory landscape underlying antiviral immunity in a farmed fish with a complex genome.**

[Supplemental material is available for this article.]

The innate immune response to viral infection, which is mainly based on the type I interferon (IFN) pathway, is crucial to both disease progression and the outcome of infection. Type I IFNs are present in all gnathostomes and play a pivotal role in inducing an antiviral state in host responding cells by the induction of IFN-stimulated genes (ISGs) (Schoggins 2019).

This antiviral response is triggered when viral pathogen-associated molecular patterns (PAMPs) bind to pattern recognition receptors (PRRs) such as toll-like receptors (TLR3, TLR7, TLR8) and RIG-I-like receptors (RLRs), activating downstream signaling cascades that induce transcription of type I IFNs and antiviral effectors (Thompson et al. 2011). In mammals, teleost fish, and other vertebrate species, this response is regulated at multiple levels, including complex transcriptional feedback loops and chromatin-mediated control of key antiviral genes (Ivashkiv and Donlin 2014; Dehler et al. 2019). Epigenetic modifications such as histone acetylation and methylation contribute to this regulation by altering DNA accessibility at enhancers and promoters (Mostafavi et al. 2016; Kan et al. 2022). Transposase-accessible chromatin with sequencing (ATAC-seq) and chromatin immunoprecipitation and sequencing (ChIP-seq) are widely used to map open chromatin and histone modifications across the genome, enabling the identification of putative regulatory elements. Although these assays are powerful, they have limitations, including the potential for false positives (regions that are accessible but not functionally active) and false negatives (context-dependent enhancers that may be missed in bulk analysis). Nonetheless, ATAC-seq and ChIP-seq have proven effective in both mammalian and teleost systems for revealing the epigenomic architecture of immune tissues and mapping regulatory elements associated with IFN responses (Cooper et al. 2024; Harvey et al. 2024; Tan et al. 2025).

The induction of type I IFN typically involves an initial detection and recognition of viral RNA by cytoplasmic RNA helicases like RIG-I and interferon induced with helicase C domain 1 (IFIH1 [also known as MDA5]) or TLRs (TLR3, TLR7/8) (Matsumoto et al. 2003; Liu 2005). In the human or mouse, this leads to the production and secretion of IFNA and IFNB, which then bind to their cognate receptors, interferon alpha and beta receptor subunit 1 (IFNAR1) and interferon alpha and beta receptor subunit 2 (IFNAR2) present on the surface of target cells. Activation of these receptors induces a signaling cascade, leading to the phosphorylation of the Janus kinases TYK2 and JAK1, as well as the signal transducer and activator of transcription 1 and 2 (STAT1 and STAT2) (Platanias 2005). These phosphorylated

**Corresponding authors: sam.martin@abdn.ac.uk, pierre.boudinot@inrae.fr**

Article published online before print. Article, supplemental material, and publication date are at https://www.genome.org/cgi/doi/10.1101/gr.280579.125. Freely available online through the *Genome Research* Open Access option.

© 2026 Naseer et al. This article, published in *Genome Research*, is available under a Creative Commons License (Attribution-NonCommercial 4.0 International), as described at http://creativecommons.org/licenses/by-nc/4.0/.

Downloaded from genome.cshlp.org on November 17, 2026 . Published by Cold Spring Harbor Laboratory Press



STAT1 and STAT2 molecules then bind with a third subunit, interferon regulatory factor 9 (IRF9), to form the IFN-stimulated gene factor 3 (ISGF3) complex (Platanitis et al. 2019). After translocation to the cell's nucleus, ISGF3 binds to IFN-stimulated response elements (ISRE) in the promotors of ISGs, rapidly activating diverse genes with effector and regulatory immune function (Platanias 2005; Ivashkiv and Donlin 2014). The binding of ISGF3 to ISREs is essential for the induction of ISGs and the establishment of an antiviral cellular state (Wang et al. 2017). Multiple type I IFNs are present in and orchestrate antiviral innate responses teleost fish (Langevin et al. 2019). The ISG repertoire is more complex compared with mammals, with additional gene family member paralogs being retained following whole-genome duplication (WGD) events (Collet et al. 2009; Skjesol et al. 2010; Briolat and Johnston 2014; Macqueen and Johnston 2014; Levraud et al. 2019; Gan et al. 2020; Clark et al. 2023). In addition to the presence of mammalian orthologs and their paralogous genes resulting from WGD, several gene families involved in antiviral immunity, such as GCRV-induced gene 1 (gig1), RNA-dependent protein kinase (pkr/pkz), and specific TRIM gene subsets such as finTRIMs, are unique to teleost fish. These teleost-specific ISGs likely evolved during lineage-specific expansions and are thought to play important roles in shaping fish-specific IFN responses or could have been lost in the lineages leading to tetrapods (Levraud et al. 2019; An et al. 2025).

Although the teleost IFN response has been extensively analyzed at the transcriptomic level (e.g., Martin et al. 2007; Zou and Secombes 2011; Briolat et al. 2014; Levraud et al. 2019; Clark et al. 2023) and functionality of ISREs has been proposed (Boudinot et al. 2001; Collet and Secombes 2001; Castro et al. 2008, 2010), the regulatory basis of the IFN system, and, more generally, antiviral transcriptional responses, remains poorly understood. To tackle this knowledge gap, we investigated the genomic regulatory mechanisms driving core ISG expression responses in the head kidney of Atlantic salmon (*Salmo salar*), a globally important aquaculture species.

We hypothesised that (1) gene regulation in response to polyinosinic:polycytidylic acid (poly I:C) stimulation involves coordinated changes in chromatin accessibility and histone modifications, similar to mechanisms described in higher vertebrates; (2) regulatory divergence between paralogous genes contributes to their differential expression during the antiviral response; and (3) expanded or salmonid-specific gene families exhibit distinct regulatory signatures that reflect their functional roles in immunity.

To test these hypotheses, we integrated ATAC-seq, ChIP-seq, and RNA-seq data sets following in vivo stimulation with the viral dsRNA mimic poly I:C. ChIP-seq was performed using the histone marks H3K27ac and H3K27me3. H3K27ac is an activating mark associated with open chromatin and transcriptionally active genes, marking promoter and enhancer regions (Wang et al. 2008; Creyghton et al. 2010). In contrast, H3K27me3 is a repressive mark associated with polycomb-mediated transcriptional repression and gene silencing (Bernstein et al. 2006; Barski et al. 2007), typically associated with regulatory regions of inactive genes. As salmonid genomes are characterized by two rounds of WGD (Lien et al. 2016; Robertson et al. 2017), leading to the expansion and functional diversification of many gene sets compared with mammals (including ISGs) (Clark et al. 2023), we further compared the regulation of ISG paralogs to seek evidence for changes in regulation or function. Our findings advance understanding of immune function, providing insights into the evolution of teleost fish paralogous ISGs at the regulatory level, while demonstrating functional conservation of key antiviral regulatory elements across vertebrates.

## Results

In this study, we examine the modulation of gene expression, chromatin accessibility, and histone modifications in Atlantic salmon following stimulation using poly I:C, a mimic of infection with an RNA virus. A major transcriptomic response was elicited driving the upregulation of a core set of ISGs (Clark et al. 2023). In this report, we use the term ISGs to include all genes inducible within the IFN response, including those that are directly upregulated by poly I:C stimulation. The aim of the current study is to elucidate epigenomic changes in chromatin state following this stimulation and shed light on regulatory elements and transcription factor binding sites (TFBSs) influencing antiviral transcriptional responses in a complex teleost genome.

### Genomic sequencing data and sample metadata

Thirty-eight data sets were generated, comprising ATAC-seq (12 data sets: $n = 6$ poly I:C, $n = 6$ PBS control) and ChIP-seq (12 data sets per histone mark: $n = 6$ poly I:C, $n = 6$ PBS; along with two input controls). For H3K27ac, one PBS sample was excluded from the analysis postsequencing, whereas for H3K27me3, one sample each for PBS and poly I:C was excluded. Full details regarding samples and sequence data are provided in Supplemental Table 1. ATAC-seq provides genome-wide identification of open chromatin regions and, with six controls and six poly I:C–stimulated fish, offers in-depth data to study regulatory elements, TFBSs, and changes in chromatin accessibility. ChIP-seq was performed using two histone modifications: H3K27ac and H3K27me3. Promoters and enhancers were defined based on chromatin accessibility, histone modifications, and ChromHMM annotations. Regions classified as putative promoters were those overlapping transcription start sites (TSSs) with ATAC-seq consensus peaks and H3K27ac enrichment, indicative of active regulatory activity. Specifically, candidate enhancers were identified as intergenic or intronic regions that exhibited both ATAC-seq accessibility and H3K27ac modification, suggesting distal regulatory elements. Peaks marked predominantly by H3K27me3 were classified as polycomb-repressed regions, reflecting transcriptionally silent chromatin states. These ChromHMM-annotated enhancers and promoters, defined through the integration of ATAC-seq and H3K27ac, were subsequently used for downstream TFBS analysis, allowing the identification of key regulatory motifs involved in the antiviral response.

To further characterize the genomic distribution of ATAC-seq and H3K27ac peaks, we annotated consensus peaks relative to gene features and TSSs. The majority of peaks in both the ATAC-seq and H3K27ac data sets were associated with genes (Fig. 1A,B) and enriched in promoter-proximal and enhancer regions, with a high density observed within 50 kb of the TSS (Fig. 1C,D). This confirms the utility of these data sets for identifying active regulatory elements in the Atlantic salmon genome.

### Immune stimulation remodels chromatin accessibility and histone modifications in Atlantic Salmon head kidney

The poly I:C stimulation led to widespread changes in chromatin accessibility, with an ~25% increase in ATAC-seq peaks detected in treated fish (53,102 ± 6142) compared with the PBS controls (39,869 ± 11,858). These accessible regions were distributed across

Downloaded from genome.cshlp.org on November 17, 2026 . Published by Cold Spring Harbor Laboratory Press



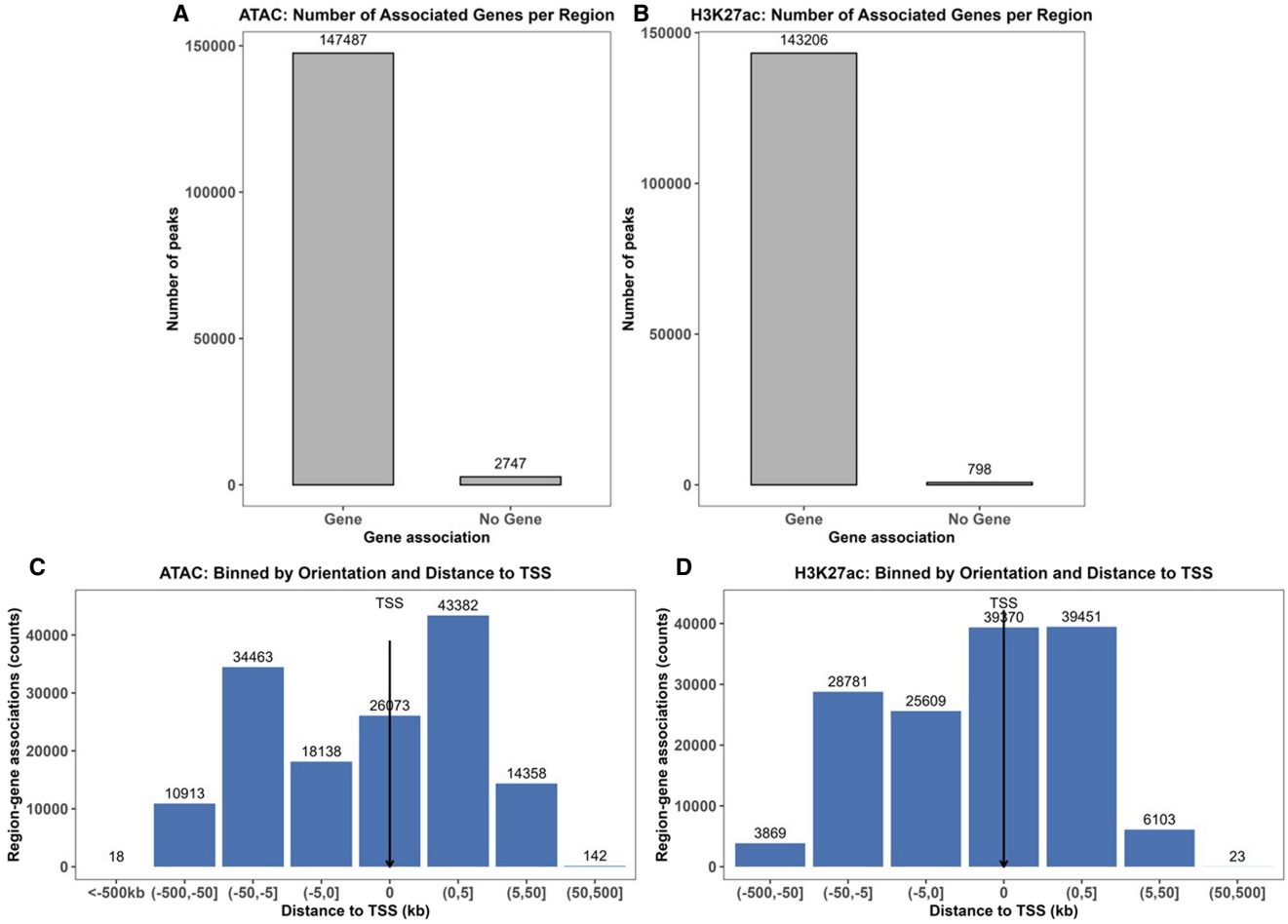



**Figure 1.** Genomic distribution of ATAC-seq and H3K27ac ChIP-seq peaks relative to gene features and transcription start sites (TSSs). (*A*,*B*) Barplots showing the number of consensus peaks associated or unassociated with genes in the ATAC-seq (*A*) and H3K27ac (*B*) data sets. (*C*,*D*) Distribution of peak–gene associations binned by signed distance to the nearest TSS in the ATAC-seq (*C*) and H3K27ac (*D*) data sets. Most peaks are located within 50 kb of a TSS, supporting their annotation as promoters or enhancers.

promoter-TSS (10%), exonic (13%), intronic (45%), and intergenic (26%) features of the genome (Supplemental Fig. 2A). To illustrate the data quality and consistency, genome browser tracks at the housekeeping gene *elf1a* showed well-defined *cis*-regulatory peaks in both conditions, matching the expected expression patterns (Fig. 2A,B).

Differential analysis identified 613 regions (250 promoters, 363 enhancers) with increased accessibility and 48 regions (six promoters, 42 enhancers) with reduced accessibility after poly I:C stimulation (fold change > 2, *P*adj < 0.05) (Fig. 2E; Supplemental Table 2). Functional enrichment of the regions with increased accessibility, performed using rGREAT, highlighted pathways central to antiviral immunity, including "*regulation of cytokine-mediated signaling*," "*interferon-mediated signaling*," and "*type I interferon response*" (Fig. 2C; Supplemental Table 3A). Several terms related to JAK-STAT signaling and host–virus interactions were also among the top enriched categories.

Chromatin immunoprecipitation profiling of H3K27ac and H3K27me3 marks further revealed distinct patterns of histone modification following immune stimulation. Stimulated fish showed an average of 72,490 (±21,211) H3K27ac and 68,873 (±16,608) H3K27me3 peaks compared with 78,816 (±31,106) and 48,221 (±26,905) in PBS controls. Analysis of differential abundance identified 1539 regions enriched for H3K27ac (528 promoters, 1011 enhancers) and 794 regions enriched for H3K27me3 (124 promoters, 670 enhancers), although a comparable number of regions were lost for each respective mark in response to stimulation (Fig. 2F,G; Supplemental Table 4). A small subset of loci (45) exhibited reciprocal regulation, gaining H3K27ac while losing H3K27me3, suggesting polycomb-mediated repression was relieved to allow gene activation (Supplemental Fig. 3C; Supplemental Table 5). In contrast, only 30 regions showed concurrent increases in both marks, supporting the notion that their regulation is largely independent in this context (Supplemental Fig. 3A).

Gene set enrichment of regions gaining H3K27ac underscored their association with immune processes, including "interferon-mediated signaling," "cellular response to type I interferon," "response to virus," and pathways involved in epithelial and endothelial cell migration (Fig. 2D; Supplemental Fig. 3B). Comparison of the enriched biological processes revealed that eight out of the top 15 Gene Ontology (GO) terms identified in ATAC-seq peaks were also significantly enriched among regions gaining H3K27ac. These shared terms included hallmark antiviral

Downloaded from genome.cshlp.org on November 17, 2026 . Published by Cold Spring Harbor Laboratory Press



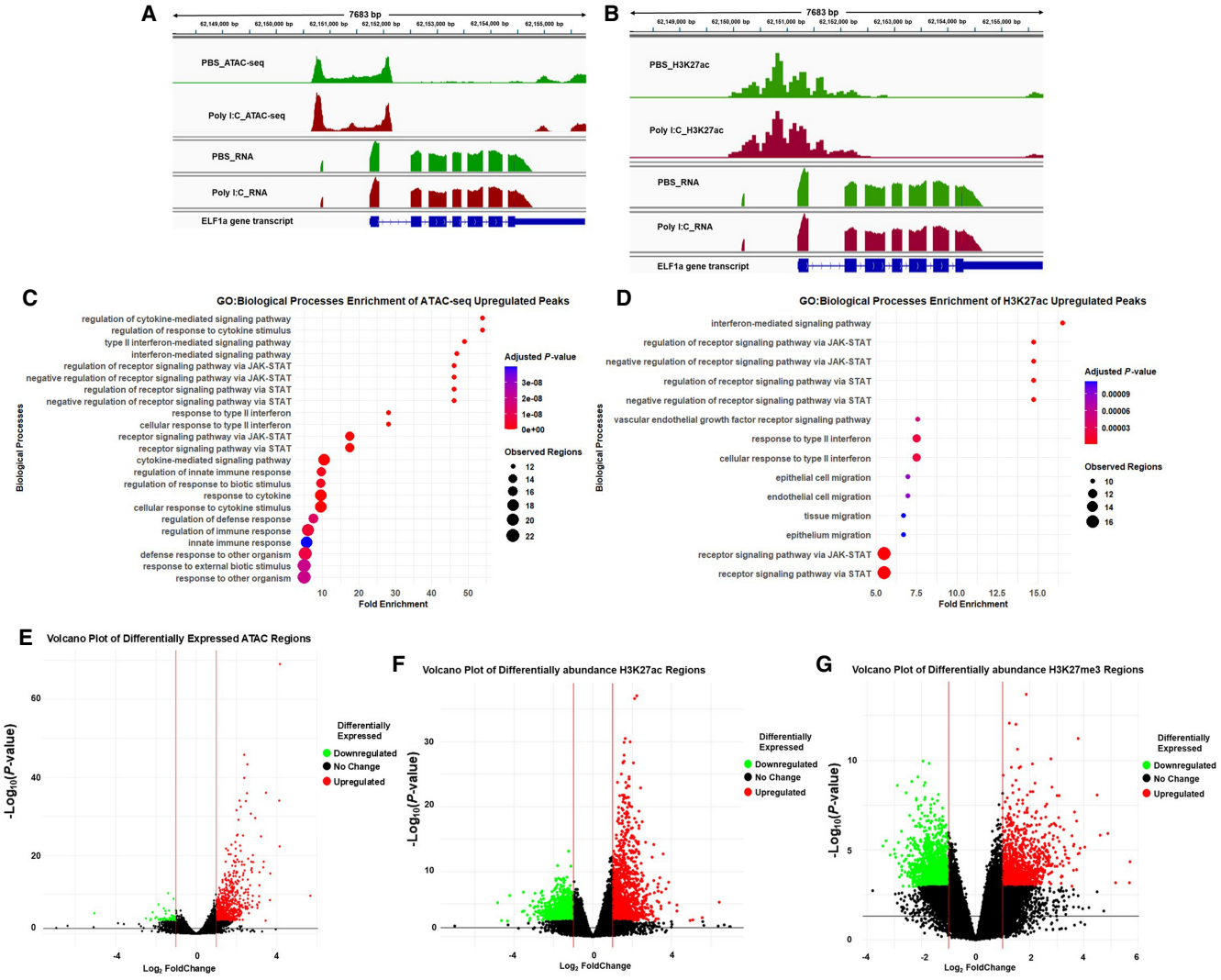



**Figure 2.** Integrative analysis of chromatin accessibility, histone modifications, and gene expression following poly I:C stimulation in Atlantic salmon. (*A*) Genome browser tracks showing ATAC-seq, RNA-seq, and gene annotation at the *elf1a* locus in PBS (control) and poly I:C–stimulated samples. The housekeeping gene *elf1a* is shown as a representative locus to illustrate the data quality and consistency across assays. (*B*) Genome browser tracks at the same locus showing H3K27ac ChIP-seq signal, indicating histone modification in both control and poly I:C–stimulated samples. (*C*) Gene Ontology (GO) biological process enrichment of genes associated with upregulated ATAC-seq peaks. Dot size reflects the number of observed regions; color scale indicates adjusted *P*-values. (*D*) GO biological process enrichment of genes associated with upregulated H3K27ac peaks, displayed as in *C*. For GO analysis, the following filtrations were carried out: fold enrichment greater than five, observed hits of 10 or more, and *P*-adjusted < 0.05. (*E*) Volcano plot of differentially accessible ATAC-seq regions between PBS and poly I:C. Red points indicate significantly upregulated regions, green points indicate downregulated regions, and black points are not significant. (*F*) Volcano plot of differentially enriched H3K27ac-marked regions. (*G*) Volcano plot of differentially enriched H3K27me3-marked regions.

processes such as "interferon-mediated signaling pathway," "response to type I interferon," and "regulation of receptor signaling pathway via JAK-STAT," reflecting coordinated chromatin accessibility and histone acetylation at critical immune loci. These findings demonstrate a coordinated regulatory response to poly I:C, involving both chromatin accessibility and activating histone modifications at key antiviral loci.

## Multiomics identify epigenomic changes associated with the induction of core ISGs

To uncover the regulatory mechanisms underlying the transcriptome response induced by poly I:C, we integrated data from RNA-seq, ATAC-seq, and ChIP-seq for the active histone mark H3K27ac and repressive histone mark H3K27me3. For this analysis, we defined 3541 genes associated with changes across all four assays, split into five subsets with distinct regulatory profiles (Fig. 3A). Of interest, we find different groups of genes that are activated at different levels, these are, first, core genes (197 genes; set 1) were defined by significant concurrent increases in ATAC-seq chromatin accessibility, H3K27ac signal, and mRNA expression following poly I:C stimulation. The presence of both open chromatin regions and H3K27 acetylation close to these genes suggests that these regions function as candidate active enhancers and promoters, driving transcriptional activation in response to stimulation (Fig. 3B). The second gene set (1348 genes; set 2) exhibited

Downloaded from genome.cshlp.org on November 17, 2026 . Published by Cold Spring Harbor Laboratory Press



significant increases in chromatin accessibility and H3K27ac signal without corresponding transcriptional upregulation. These regions likely represent candidate active enhancers and promoters that are primed for activation but may require additional regulatory inputs for transcriptional induction (Fig. 3C). Third are genes that show increased mRNA expression but lack changes in chromatin accessibility (1008 genes; set 3) (Fig. 3D). Fourth are genes that show increased mRNA expression and chromatin openness but lack changes in H3K27ac signal (52 genes; set 4) (Fig. 3E), and fifth are genes with significant increases in H3K27ac signals alongside transcript-level upregulation (173 genes; set 5) (Fig. 3F; Supplemental Table 6). Canonical antiviral genes were mainly enriched in set 1, which exhibited coordinated increases in gene expression, chromatin accessibility, and H3K27ac. This group included key effectors such as *TRIM25*, *RSAD2*, *IRF7*, *MX1*, and *IFI44*. Additional antiviral genes, such as *STAT1* and *IRF8*, were found in set 3 (RNA-seq only). Few antiviral genes were detected in sets 2, 4, or 5, underscoring set 1 as the principal group reflecting multilayered antiviral gene regulation.

The core 197 genes (set 1 above) displayed increases in chromatin openness and H3K27ac signal alongside significant transcript upregulation, underscoring their tight regulatory

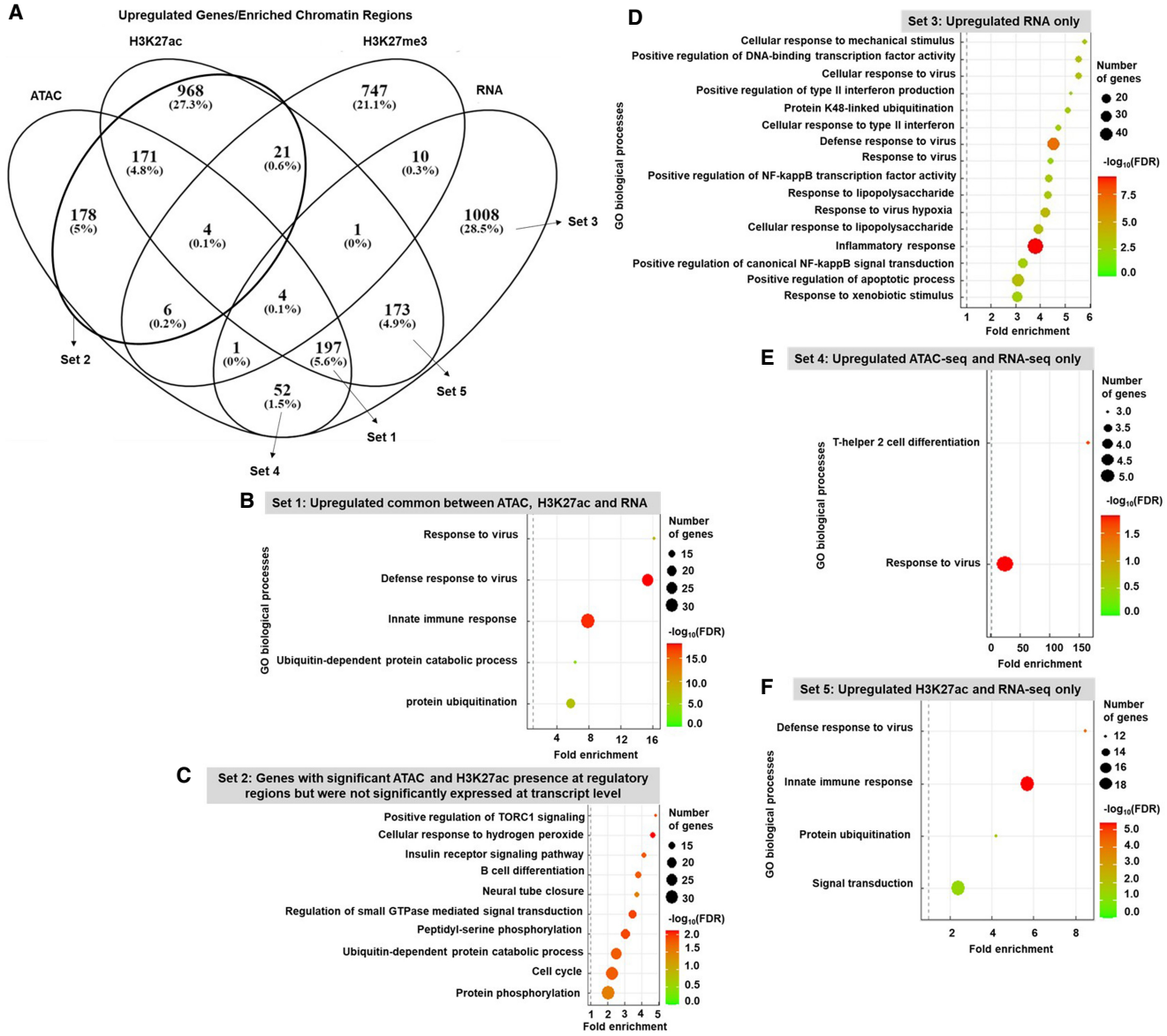



**Figure 3.** Comparative analysis of the ATAC, ChIP, and RNA-seq data following poly I:C–stimulated Atlantic salmon. (*A*) Venn diagram illustrating the overlap of upregulated genes among the different assays. (*B*) Gene Ontology (GO) analysis of the upregulated genes shared between ATAC, RNA-seq, and ChIP H3K27ac, providing insights into the biological processes associated with these genes and their involvement in the antiviral response. (*C*) Genes that had significant ATAC and H3K27ac presence at regulatory regions but were not significantly expressed at transcript level. (*D*) Genes that were upregulated at transcript level; however, their regulatory regions were not significantly activated. (*E*) Genes that were significantly expressed and had significantly increased accessible ATAC peaks. (*F*) Genes that were significantly expressed and had significant H3K27ac peaks. GO analysis was performed using DAVID, with stringent filtering criteria of FDR < 0.05 and fold enrichment greater than two.

Downloaded from genome.cshlp.org on November 17, 2026 . Published by Cold Spring Harbor Laboratory Press



coordination. Functional enrichment for GO terms revealed these genes are primarily involved in early innate immune responses, with significant enrichment for terms such as "*response to virus*," "*innate immune response*," and "*protein ubiquitination*" (Fig. 3B). Importantly, further analysis of this subset revealed that 54 (27%) of the 197 genes overlapped with the core set of Atlantic salmon ISG induced in vivo that is conserved between salmon and human (154 genes) (Supplemental Fig. 4; Table 1; Clark et al. 2023). This is significantly higher (two-tailed Fisher's exact test, $P < 0.0001$) than the conserved ISG proportion among all poly I:C–induced genes (154 out of 1446 transcriptionally induced genes, i.e., 11%), this evolutionary conservation underscores the central importance of these genes in antiviral immunity.

A subset of 1348 genes (set 2 above) showed significant increases in chromatin accessibility and H3K27ac signal without corresponding changes in transcript levels. To further investigate this finding, we analyzed the genomic context of the associated peaks. Many peaks were located in intergenic or intronic regions, indicative of putative enhancers. As enhancers often regulate distal genes rather than the closest annotated gene, this could explain the absence of detectable changes in RNA levels for nearby loci. For peaks associated with promoters, the increased chromatin accessibility and H3K27ac signal may reflect transcriptional activation that is not captured in total RNA-seq data. This could occur if small transcriptional changes are masked by the stability and abundance of pre-existing transcripts in the cytoplasm. The corresponding gene set did not exhibit enrichment for antiviral or IFN-response pathways, suggesting potential involvement in alternative biological processes (Fig. 3C).

Third, we identified a subset of genes (set 3 above) that were differentially expressed in response to poly I:C but did not exhibit changes in chromatin accessibility or histone mark modifications. These genes were enriched for GO terms such as "*cellular response to virus*," "*positive regulation of NF-kappaB transcription factor activity*," "*response to lipopolysaccharide*," "*cellular response to type II interferon*," and "*inflammatory response*" (Fig. 3D), highlighting their pivotal role in the antiviral response.

Fourth, we identified a set of 52 genes (set 4 above) that exhibited significant changes in chromatin accessibility and transcript levels, without corresponding alterations in H3K27ac marks. GO term enrichment for these genes included "*T-helper 2 cell differentiation*" and "*response to virus*" (Fig. 3E). The lack of H3K27ac changes suggests that these genes might be regulated through distal enhancers, changes in chromatin topology, or mechanisms unrelated to histone acetylation.

Fifth, a distinct set of 173 genes showed significant increases in H3K27ac signals alongside transcript-level upregulation, but no ATAC-seq signal. These genes were enriched for GO terms such as "*defense response to virus*," "*innate immune response*," "*protein ubiquitination*," and "*signal transduction*" (Fig. 3F), reflecting their active involvement in the antiviral response. The concurrent increase in H3K27ac and gene expression strongly supports their role as actively transcribed loci, with acetylation marking a key feature of them in response to poly I:C stimulation.

Finally, a subset of 747 genes was exclusively associated with increase in repressive histone mark H3K27me3, which is typically linked to transcriptional silencing through repressive polycomb complexes, with known roles in regulating immune responses (Bosselut 2016). However, GO analysis did not reveal any significantly enriched terms for this subset, indicating a lack of strong functional enrichment for these genes.

## A key ISRE motif, IRF8 drives the antiviral gene regulatory network

To further investigate regulatory mechanisms driving the antiviral response, we focused on the core set of 197 genes identified above showing coordinated changes in expression, chromatin accessibility, and H3K27ac signal. TFBS enrichment analysis was performed on the peaks or regions corresponding to those 197 genes containing both enhancers and promoters, which revealed nine enriched TFBSs (Fig. 4A). The most enriched TFBS was IFN regulatory factor 8 (IRF8), a highly characterized binding site used during IFN responses (Mancino et al. 2015). The IRF8 binding site was identified in the regulatory regions of 37 of the 197 genes (18.8%), and all these genes were also highly significantly upregulated at the mRNA level, supporting the functional relevance of IRF8 motif enrichment in the antiviral response (Table 2). The IRF8 binding site corresponds to the ISRE, a motif that has core elements of nnGAAAnnGAAAnn (Fig. 4B) shared with many other ISRE elements found in or near IFN-responsive genes (Tamura et al. 2015). This ISG subset includes key antiviral effectors such as *MX*, an IFN-inducible dynamin-like large GTPases that is well characterized to mediate antiviral activities; a TRIM ubiquitin ligase involved in viral neutralization; *MEFV*, a key regulator of innate immunity; and *PARP14*, a poly(ADP-ribose) polymerase involved in transcriptional activation of ISGs (Haller et al. 2007; Caprara et al. 2018; Koepke et al. 2021). The TFBS motif for IRF8-binding motifs (Fig. 4B) confirms the functional conservation of the ISRE sequence, consistent with its binding preferences and regulatory function in ISGs. These findings are consistent with the earlier observation of GO term enrichment for the 197 genes (Fig. 3B), which were associated with processes such as "*response to virus*" and "*innate immune response*". The prevalence of IRF8 motifs within these genes further supports this transcription factor's role as a critical transcription factor driving IFN-stimulated regulatory networks during poly I:C stimulation.

## Chromatin-state dynamics and TFBS analyses using whole ATAC-seq and ChIP-seq data sets

To investigate the chromatin landscape underlying the antiviral immune response to poly I:C, we applied ChromHMM modelling to the ATAC-seq, H3K27ac, and H3K27me3 data sets. This integrative analysis identified five distinct chromatin states, annotated following the framework established by Ernst and Kellis (2017; Fig. 5A–C). These chromatin states were classified as follows: (1) ATAC Islands are regions characterized by high chromatin accessibility, indicative of active regulatory activity lacking H3K27ac and H3K27me3 and the presence of potential enhancer or promoter elements; (2) quiescent/low regions are areas with minimal chromatin accessibility and low regulatory activity, suggesting these regions are largely inactive under the conditions tested; (3) repressed states are regions dominated by H3K27me3 with low ATAC-seq signal, indicative of transcriptional silencing mediated by polycomb repression; and (4) poised enhancer states are regions marked by H3K27me3 (repressive mark) alongside H3K4me1, indicative of enhancers that are primed but not yet active. These regions may transition to an active state upon specific stimuli through the loss of H3K27me3 and the acquisition of H3K27ac, which marks active enhancers (Barral and Déjardin 2023). Fifth are active regulatory elements (enhancers/promoters), which are regions displaying strong ATAC-seq and H3K27ac signals, reflecting robust regulatory activity and heightened chromatin accessibility at enhancers and promoters. ChromHMM analysis

Downloaded from genome.cshlp.org on November 17, 2026 . Published by Cold Spring Harbor Laboratory Press



**Table 1.** 54 conserved ISGs common between ATAC-seq, ChIP-seq (H3K27ac), and RNA-seq

| Ensembl id | FC ATAC | FC H3K27ac | FC RNA | HGNC | Gene name |
|---|---|---|---|---|---|
| ENSSSAG00000068365 | 4.16 | 1.62 | 5.64 | *IFIT5* | interferon induced protein with tetratricopeptide repeats 5 |
| ENSSSAG00000064740 | 3.35 | 2.16 | 4.49 | *UBB* | ubiquitin B |
| ENSSSAG00000077530 | 2.79 | 2.35 | 4.58 | *MX1* | MX dynamin like GTPase 1 |
| ENSSSAG00000041408 | 2.75 | 3.29 | 4.12 | *RNF213* | ring finger protein 213 |
| ENSSSAG00000043101 | 2.72 | 1.62 | 5.39 | *BATF* | Basic Leucine Zipper ATF-Like Transcription Factor |
| ENSSSAG00000108395 | 2.58 | 3.09 | 4.54 | *SAMD9* | sterile alpha motif domain containing 9 |
| ENSSSAG00000118579 | 2.55 | 3.88 | 4.88 | *SOCS1* | suppressor of cytokine signaling 1 |
| ENSSSAG00000104513 | 2.44 | 3.46 | 4.79 | *SOCS1* | suppressor of cytokine signaling 1 |
| ENSSSAG00000043265 | 2.40 | 1.84 | 4.91 | *HERC3* | HECT and RLD domain containing E3 ubiquitin protein ligase 3 |
| ENSSSAG00000007886 | 2.39 | 2.24 | 5.22 | *CMPK2* | cytidine/uridine monophosphate kinase 2 |
| ENSSSAG00000073332 | 2.21 | 1.55 | 3.01 | *HELZ2* | helicase with zinc finger 2 |
| ENSSSAG00000121778 | 2.04 | 1.12 | 5.49 | *UBB* | ubiquitin B |
| ENSSSAG00000058932 | 2.02 | 1.95 | 3.22 | *PARP14* | poly(ADP-ribose) polymerase family member 14 |
| ENSSSAG00000078539 | 2.02 | 1.55 | 1.66 | *RNF213* | ring finger protein 213 |
| ENSSSAG00000056446 | 1.98 | 1.86 | 3.79 | *NLRC5* | NLR family CARD domain containing 5 |
| ENSSSAG00000077480 | 1.96 | 1.71 | 4.64 | *NAMPT* | nicotinamide phosphoribosyltransferase |
| ENSSSAG00000043036 | 1.94 | 1.54 | 4.24 | *ZNFX1* | zinc finger NFX1-type containing 1 |
| ENSSSAG00000075304 | 1.92 | 1.69 | 2.98 | *EIF2AK2* | eukaryotic translation initiation factor 2 alpha kinase 2 |
| ENSSSAG00000005181 | 1.85 | 1.48 | 3.31 | *SAMD9L* | sterile alpha motif domain containing 9 like |
| ENSSSAG00000054938 | 1.82 | 1.85 | 2.51 | *PARP12* | poly(ADP-ribose) polymerase family member 12 |
| ENSSSAG00000071823 | 1.77 | 2.65 | 2.48 | *XCL2* | X-C motif chemokine ligand 2 |
| ENSSSAG00000110347 | 1.77 | 1.32 | 5.65 | *TREX1* | three prime repair exonuclease 1 |
| ENSSSAG00000079036 | 1.74 | 2.05 | 4.92 | *IFIT5* | interferon induced protein with tetratricopeptide repeats 5 |
| ENSSSAG00000072910 | 1.70 | 2.31 | 3.17 | *IFI44L* | interferon induced protein 44 like |
| ENSSSAG00000068298 | 1.66 | 1.59 | 1.48 | *NLRC5* | NLR family CARD domain containing 5 |
| ENSSSAG00000059637 | 1.65 | 1.19 | 1.75 | *TSPAN33* | tetraspanin 33 |
| ENSSSAG00000004551 | 1.63 | 1.74 | 3.08 | *XAF1* | XIAP associated factor 1 |
| ENSSSAG00000003156 | 1.62 | 1.66 | 5.13 | *RIGI* | retinoic acid-inducible gene I |
| ENSSSAG00000075036 | 1.62 | 2.35 | 3.40 | *LGALS3BP* | galectin 3 binding protein |
| ENSSSAG00000081672 | 1.61 | 1.21 | 3.48 | *PARP9* | poly(ADP-ribose) polymerase family member 9 |
| ENSSSAG00000049790 | 1.55 | 1.82 | 3.25 | *LGALS9C* | galectin 9C |
| ENSSSAG00000046065 | 1.53 | 1.59 | 3.50 | *USP20* | ubiquitin specific peptidase 20 |
| ENSSSAG00000051388 | 1.52 | 1.69 | 4.17 | *NCOA7* | nuclear receptor coactivator 7 |
| ENSSSAG00000005381 | 1.51 | 2.31 | 3.94 | *PARP12* | poly(ADP-ribose) polymerase family member 12 |
| ENSSSAG00000078885 | 1.48 | 1.48 | 2.73 | *IFIH1* | interferon induced with helicase C domain 1 |
| ENSSSAG00000119673 | 1.47 | 1.64 | 2.54 | *RIGI* | retinoic acid-inducible gene I |
| ENSSSAG00000072880 | 1.46 | 1.82 | 2.93 | *TRAFD1* | TRAF-type zinc finger domain containing 1 |
| ENSSSAG00000054674 | 1.46 | 1.43 | 1.88 | *RNF213* | ring finger protein 213 |
| ENSSSAG00000045256 | 1.45 | 1.18 | 2.69 | *IFI44* | interferon induced protein 44 |
| ENSSSAG00000045959 | 1.45 | 1.69 | 1.94 | *PARP12* | poly(ADP-ribose) polymerase family member 12 |
| ENSSSAG00000048046 | 1.36 | 1.39 | 6.43 | *RSAD2* | radical S-adenosyl methionine domain containing 2 |
| ENSSSAG00000020083 | 1.34 | 1.84 | 2.96 | *PARP12* | poly(ADP-ribose) polymerase family member 12 |
| ENSSSAG00000002526 | 1.28 | 1.36 | 2.92 | *USP20* | ubiquitin specific peptidase 20 |
| ENSSSAG00000077407 | 1.26 | 1.25 | 1.53 | *TAPBP* | TAP binding protein |
| ENSSSAG00000042163 | 1.22 | 1.77 | 2.42 | *PARP9* | poly(ADP-ribose) polymerase family member 9 |
| ENSSSAG00000037936 | 1.15 | 2.03 | 1.49 | *LGALS3BP* | galectin 3 binding protein |
| ENSSSAG00000119808 | 1.14 | 1.68 | 2.13 | *OGFR* | opioid growth factor receptor |
| ENSSSAG00000006364 | 1.12 | 1.65 | 1.76 | *ADAR* | adenosine deaminase RNA specific |

(*continued*)

Downloaded from genome.cshlp.org on November 17, 2026 . Published by Cold Spring Harbor Laboratory Press



**Table 1.** *Continued*

| Ensembl id | FC ATAC | FC H3K27ac | FC RNA | HGNC | Gene name |
|---|---|---|---|---|---|
| ENSSSAG00000001032 | 1.11 | 1.50 | 1.94 | *RNF114* | ring finger protein 114 |
| ENSSSAG00000076373 | 1.08 | 1.75 | 3.37 | *IRF7* | interferon regulatory factor 7 |
| ENSSSAG00000074138 | 1.06 | 1.17 | 2.29 | *CGAS* | cyclic GMP-AMP synthase |
| ENSSSAG00000058809 | 1.04 | 1.59 | 2.38 | *PARP15* | poly(ADP-ribose) polymerase family member 15 |
| ENSSSAG00000070425 | 1.03 | 1.31 | 1.31 | *MOV10* | Mov10 RISC complex RNA helicase |
| ENSSSAG00000047562 | 1.01 | 1.78 | 1.58 | *RNF213* | ring finger protein 213 |

The considered ISG data were obtained from Clark et al. (2023).

revealed that chromatin state 5, corresponding to active enhancers and promoters (enriched for ATAC-seq and H3K27ac signals), was more prevalent in poly I:C–stimulated samples compared to PBS controls (Fig. 5B,C), consistent with increased activation of regulatory regions during the antiviral response. These findings provide a high-resolution view of chromatin-state dynamics, illustrating the diversity of regulatory landscapes and their functional relevance in response to poly I:C stimulation.

To identify transcription factors potentially regulating these active regions, consensus open chromatin regions representing ChromHMM state 5 (active regulatory elements) were analyzed for TFBS enrichment (Fig. 5D). Sixteen TFBSs were either significantly enriched or underrepresented in poly I:C. Seven TFBSs were uniquely enriched in the poly I:C–stimulated group, including STAT6, IRF9, PRDM1, IRF6, JDP2, NR2E1, and BCL6. These transcription factors play central roles in antiviral immunity and immune system regulation. The presence of STAT6 (Li et al. 2016), IRF9, and IRF6 demonstrates a set of key TFBSs for IFN-responsive genes, with IRF9 sharing a binding site highly similar to that of IRF8 described earlier.

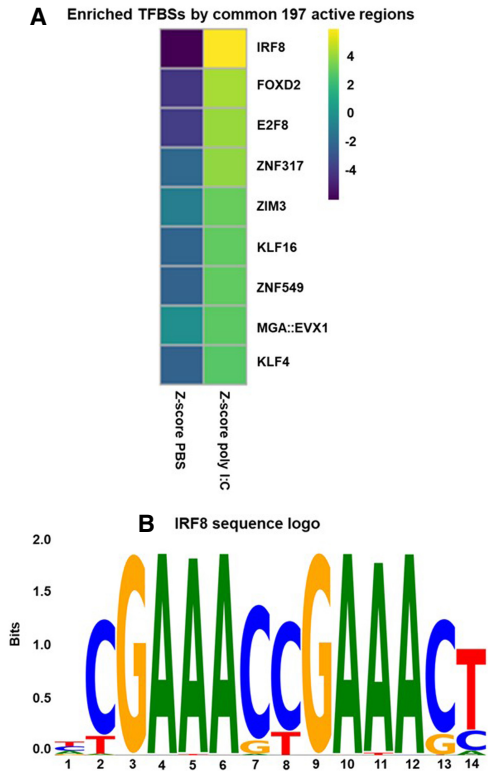



**Figure 4.** TFBS analysis of key set of antiviral genes. (*A*) TFBSs identified in a subset of 197 genes that are common among ATAC-seq, H3K27ac ChIP-seq, and RNA-seq data sets. Distribution of TFBSs showing that >20% of the genes contain IRF8 binding sites; Table 2 lists the gene IDs associated with these IRF8 binding sites. (*B*) Sequence logo representing the binding motif of IRF8, highlighting the conserved nucleotide positions crucial for IRF8 binding specificity. TFBSs were identified using GimmeMotifs from the enriched regions in ATAC-seq and H3K27ac, corresponding to active enhancers and promoters; the JASPER database was used as background.

## ISREs reside within regulatory elements driving the antiviral response

The enrichment of TFBSs for conserved vertebrate IFN regulators, including IRF3, IRF7, IRF8, IRF9, and STAT2, implies the activation of ISGs through the ISRE pathway. In this context, our focus was directed toward investigating the response induced by primary viral recognition facilitated by the RIG-I pathway, which plays a central role in initiating the IFN response and establishment of an antiviral cellular state (Fig. 6A). Specifically examining the RIG-I pathway, we observed upregulation of *rig-i*, *mda5*, *irf3*, and *irf7* at the mRNA level, with a concurrent significant increase in associated peaks in ATAC-seq and H3K27ac data sets. However, although *mavs* was expressed, as previously demonstrated, this gene was not induced by viral infection (Fig. 6B; Biacchesi et al. 2009). Notably, *rig-i* and *mda5* displayed reduced promoter H3K27me3 (repressive mark) signal in response to poly I:C, suggesting their activation rather than suppression during this immune antiviral response. Turning to the JAK-STAT pathway, we observed significant induction of the *stat1*, *stat2*, and *irf9* mRNAs, accompanied by a notable increase in promoter openness and H3K27ac signal, and a visible decrease in promoter H3K27me3 signal for *stat2* and *irf9*. These results clearly demonstrate combined chromatin activation and expression upregulation of the major signaling transcription factor genes involved in IFN and antiviral responses.

We further sought to identify ISREs within genes associated with the RIG-I and JAK-STAT pathways. Our criteria for enrichment included the presence of ISREs within promoter regions exhibiting increased accessibility and/or concurrent H3K27ac activity in response to poly I:C. Notably, *rigi* and *mda5* share the ISRE consensus sequences *TTTCGGTTTC* and *TTTCGTTTC* in their proximal promoters (Fig. 6C), whereas *irf7* and *stat1* share *TTTCACTTC* as their exclusive ISRE (Fig. 6C,D). *irf3* featured a single ISRE, *GAAAACGAAA*, whereas *stat2* and *irf9* harbor two ISREs within their proximal promoters (Fig. 6D).

We also searched for ISREs in additional key ISGs that were differentially expressed and showed increased chromatin

Downloaded from genome.cshlp.org on November 17, 2026 . Published by Cold Spring Harbor Laboratory Press



**Table 2.** Genes with enriched IRF8 (ISRE) motifs identified in a subset of 197 genes that are common among ATAC-seq, H3K27ac ChIP-seq, and RNA-seq data sets

| Ensembl ID | HGNC | Gene name | FC RNA | FDR |
|---|---|---|---|---|
| ENSSSAG00000099839 | | | 3.26 | 0.000 |
| ENSSSAG00000010621 | *EDIL3* | EGF like repeats and discoidin domains 3 | 3.33 | 0.000 |
| ENSSSAG00000044071 | *CARS1* | cysteinyl-tRNA synthetase 1 | 2.71 | 0.000 |
| ENSSSAG000c0007853 | *RNF213* | ring finger protein 213 | 3.16 | 0.000 |
| ENSSSAG00000058809 | *PARP15* | poly(ADP-ribose) polymerase family member 15 | 5.20 | 0.000 |
| ENSSSAG00000058932 | *PARP14* | poly(ADP-ribose) polymerase family member 14 | 9.32 | 0.000 |
| ENSSSAG00000004437 | *TDRD3* | tudor domain containing 3 | 12.70 | 0.000 |
| ENSSSAG00000115088 | | | 4.54 | 0.000 |
| ENSSSAG00000098558 | *MX1* | MX dynamin like GTPase 1 | 10.61 | 0.000 |
| ENSSSAG00000074112 | | | 4.95 | 0.000 |
| *ENSSSAG00000072910* | *IFI44L* | interferon induced protein 44 like | *9.01* | *0.000* |
| ENSSSAG00000112886 | *RTP4* | receptor transporter protein 4 | 35.48 | 0.000 |
| ENSSSAG00000085797 | *RTP3* | receptor transporter protein 3 | 52.11 | 0.000 |
| ENSSSAG00000045959 | *PARP12* | poly(ADP-ribose) polymerase family member 12 | 3.82 | 0.000 |
| ENSSSAG00000089774 | | | 13.42 | 0.000 |
| ENSSSAG00000061910 | *TRIM21* | tripartite motif containing 21 | 12.17 | 0.000 |
| ENSSSAG00000098931 | | | 5.49 | 0.000 |
| ENSSSAG00000032869 | *CALCOCO2* | calcium binding and coiled-coil domain 2 | 2.23 | 0.000 |
| ENSSSAG00000064740 | *UBB* | ubiquitin B | 22.54 | 0.000 |
| ENSSSAG00000121778 | *UBB* | ubiquitin B | 44.79 | 0.000 |
| ENSSSAG00000078885 | *IFIH1* | interferon induced with helicase C domain 1 | 6.64 | 0.000 |
| ENSSSAG00000074688 | | | 7.09 | 0.000 |
| ENSSSAG00000042324 | *TLR7* | toll like receptor 7 | 4.90 | 0.000 |
| ENSSSAG00000112790 | | | 2.39 | 0.000 |
| ENSSSAG00000001032 | *RNF114* | ring finger protein 114 | 3.82 | 0.000 |
| ENSSSAG00000119632 | | | 5.56 | 0.000 |
| ENSSSAG00000008629 | *HERC3* | HECT and RLD domain containing E3 ubiquitin protein ligase 3 | 3.89 | 0.000 |
| ENSSSAG00000040462 | *MEFV* | MEFV innate immunity regulator, pyrin | 5.21 | 0.000 |
| ENSSSAG00000120148 | *URGCP* | upregulator of cell proliferation | 2.88 | 0.027 |
| ENSSSAG00000053722 | *FMR1* | FMRP translational regulator 1 | 2.73 | 0.000 |
| ENSSSAG00000067713 | *ZC3H7B* | zinc finger CCCH-type containing 7B | 2.29 | 0.000 |
| ENSSSAG00000003892 | | | 11.81 | 0.001 |
| ENSSSAG00000005950 | *FRK* | fyn related Src family tyrosine kinase | 5.99 | 0.000 |
| ENSSSAG00000009694 | *TRIM35* | tripartite motif containing 35 | 18.23 | 0.000 |
| ENSSSAG00000043265 | *HERC3* | HECT and RLD domain containing E3 ubiquitin protein ligase 3 | 30.05 | 0.000 |
| ENSSSAG00000043072 | *HERC3* | HECT and RLD domain containing E3 ubiquitin protein ligase 3 | 22.19 | 0.000 |
| ENSSSAG00000063287 | *MAVS* | mitochondrial antiviral signaling protein | 8.54 | 0.000 |

(FC RNA) Fold change in response to poly I:C at mRNA level.

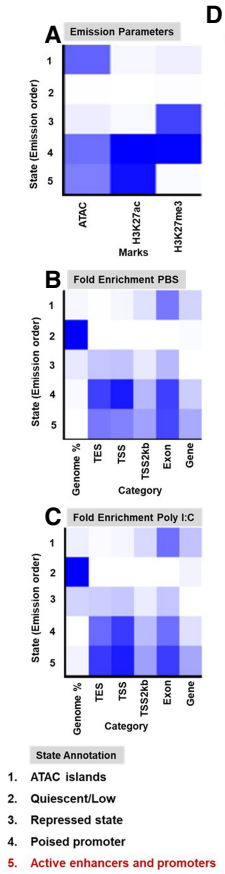
openness and H3K27ac activity upon poly I:C simulation. We focused on five genes captured in multiple enriched GO terms for antiviral activity with strong mRNA upregulation by poly I:C: *mx*, *rsad2*, *tapbp*, *isg15*, and *cd9*. ISREs were enriched in the proximal promoter of these genes, including two for *mx* (*GAAATGAAA* and *TTTCGATTTC*), two for *cd9* (*TTTCATTTC* and *TTTCTTTTC*), three for *rsad2* (*GAAACGAAA*, *TTTCGTTTTC*, and *TTTCATTTTC*), three for *tapbp* (*GAAAGGAAA*, *TTTCACTTTC*, and *TTTCATTTTT*), and one for *isg15* (*GAAACCGAAA*) (Fig. 7A,B). The peaks associated with ISRE motifs in the H3K27me3 data set either were significantly lower or remained unchanged following poly I:C stimulation, suggesting that these regions are repressed and do not undergo activation in response to the stimulus (Fig. 7B).

## ISRE enrichment is paralog specific

Salmonid fish have expanded gene families with paralogs retained from both ancestral WGDs and tandem gene duplications. Our previous work has demonstrated differential expression in response to poly I:C among paralogous ISGs (Clark et al. 2023). To further explore the regulation of these paralogs, we conducted

Downloaded from genome.cshlp.org on November 17, 2026 . Published by Cold Spring Harbor Laboratory Press






D

TFBs identified using GimmeMotifs from the enriched regions in state 5, corresponding to active enhancers and promoters

| Transcription factors | Z-score PBS | Z-score polyI:C | % with motif | Logo |
|---|---|---|---|---|
| STAT6 | -2.43 | 4.56 | 2 | |
| IRF9 | -5.39 | 4.45 | 2 | |
| PRDM1 | -2.72 | 3.89 | 2 | |
| IRF6 | -3.18 | 3.6 | 2 | |
| JDP2 | -4.04 | 3.39 | 2 | |
| NR2E1 | -1.99 | 3.09 | <1 | |
| BCL6 | -3.25 | 2.66 | <1 | |
| GATA5 | 3.34 | -1.9 | 2 | |
| ONECUT2 | 3.56 | -2.31 | 1 | |
| POU1F1 | 3.32 | -2.39 | 1 | |
| KLF9 | 3.7 | -2.68 | 2 | |
| RFX5 | 3.34 | -3.07 | 3 | |
| TBX19 | 1.66 | -3.08 | 2 | |
| ZNF93 | 2.59 | -3.17 | 2 | |
| ZSCAN4 | 4.09 | -3.38 | 2 | |
| FOXF2 | 4.15 | -4.27 | 1 | |

**Figure 5.** Transcription factor binding analysis. (*A–C*) Results of ChromHMM chromatin-state discovery using ATAC-seq and two ChIP marks (H3K27ac and H3K27me3). (*A*) The five states predicted by the model are shown and annotated based on existing literature. (*B*) The genomic location of the segments in each state is depicted for the PBS control samples. (*C*) The genomic location of the segments in each state is depicted for the poly I:C–stimulated samples. (*D*) TFBSs were identified using GimmeMotifs from the enriched regions in state 5, corresponding to active enhancers and promoters; the JASPER database was used as background. These transcription factors have binding sites enriched in ATAC and H3K27ac; however, GimmeMotif also predicted binding sites of transcription factors enriched from our data set. For the list of predicted transcription factors, refer to Supplemental Table 7.

paralog-specific ISRE motif analysis for key ISGs, including *mx*, *rsad2*, *irf9*, *irf7*, *dhx58*, *stat1*, and *cd9* (Supplemental Fig. 5).

Within the *mx* gene family, seven paralogs were identified, with four showing highly induced gene expression (ENSSSAG00000077530, ENSSSAG00000117576, ENSSSAG00000096170, and ENSSSAG00000051905) (Supplemental Fig. 5A). Notably, only the most upregulated *mx* paralog (ENSSSAG00000077530) possessed ISREs in its putative promoter (*GAAATGAAA* and *TTTCGATTTC*). Four of these *mx* paralogs are tandem repeats located on Chromosome 25.

The *rsad2* gene family is composed of four paralogs, three of which were highly upregulated by poly I:C (ENSSSAG00000048046, ENSSSAG00000108937, and ENSSSAG00000108840), each harboring two or three ISRE motifs with *GAAACGAAA* shared (Supplemental Fig. 5B). Three *rsad2* genes were found as tandem repeats on Chromosome 9, two with identified ISREs (ENSSSAG00000108840 and ENSSSAG00000108937) (Supplemental Fig. 5B).

*irf9* and *irf7* have two and three paralogs, respectively. Only one *irf9* paralog (ENSSSAG00000080439) exhibited ISRE motifs (*AAAACCGAAA* and *AAAAACGAAA*) in regulatory elements activated by poly I:C (Supplemental Fig. 5C). For *irf7*, one paralog (ENSSSAG00000076373) contained the ISRE *TTTCACTTTC* in activated regulatory elements (Supplemental Fig. 5D). A second *irf7* paralog (ENSSSAG00000066279) displayed open chromatin at the promoter, although chromatin accessibility was not significantly different between stimulated and unstimulated fish, suggesting alternative regulatory mechanisms.

The core viral receptor gene family *rigi* has three paralogs (ENSSSAG00000037858, ENSSSAG00000003156, and ENSSSAG00000119673), all showing the presence of ISREs within regulatory elements activated by poly I:C stimulation (Supplemental Fig. 5E).

In the *stat1* family, three out of five paralogs harbored ISREs in upstream regulatory regions activated by poly I:C stimulation (Supplemental Fig. 5F). One copy (ENSSSAG00000056374) had open chromatin without any ISRE, and another (ENSSSAG00000102446) did not display open chromatin in the promoter.

The *cd9* family is composed of eight paralogs, with only ENSSSAG00000059637 exhibiting ISRE regions (*TTTCATTTC* and *TTTCTTTTC*) in the proximal promoter, which was associated with the strongest mRNA expression and upregulation by poly I:C (Supplemental Fig. 5G). Four of these paralogs were identified as contigs, representing highly duplicated sequences not assignable to specific chromosomes owing to their repetitive nature.

Our paralog-specific ISRE motif analysis unveils distinct regulatory patterns and functional implications within the innate immune response, shedding light on the intricate dynamics of gene paralogs in antiviral defense mechanisms.

## Discussion

The immune response to viral infections is a fundamental aspect of host defense mechanisms conserved across vertebrates. In this study, we combined RNA-seq, ATAC-seq, and ChIP-seq to investigate the regulatory landscape underlying the antiviral response in Atlantic salmon following poly I:C stimulation, a mimic of double-stranded RNA viruses. Our aim was to elucidate the interplay between gene expression, chromatin accessibility, and histone modifications during the early stages of the immune response.

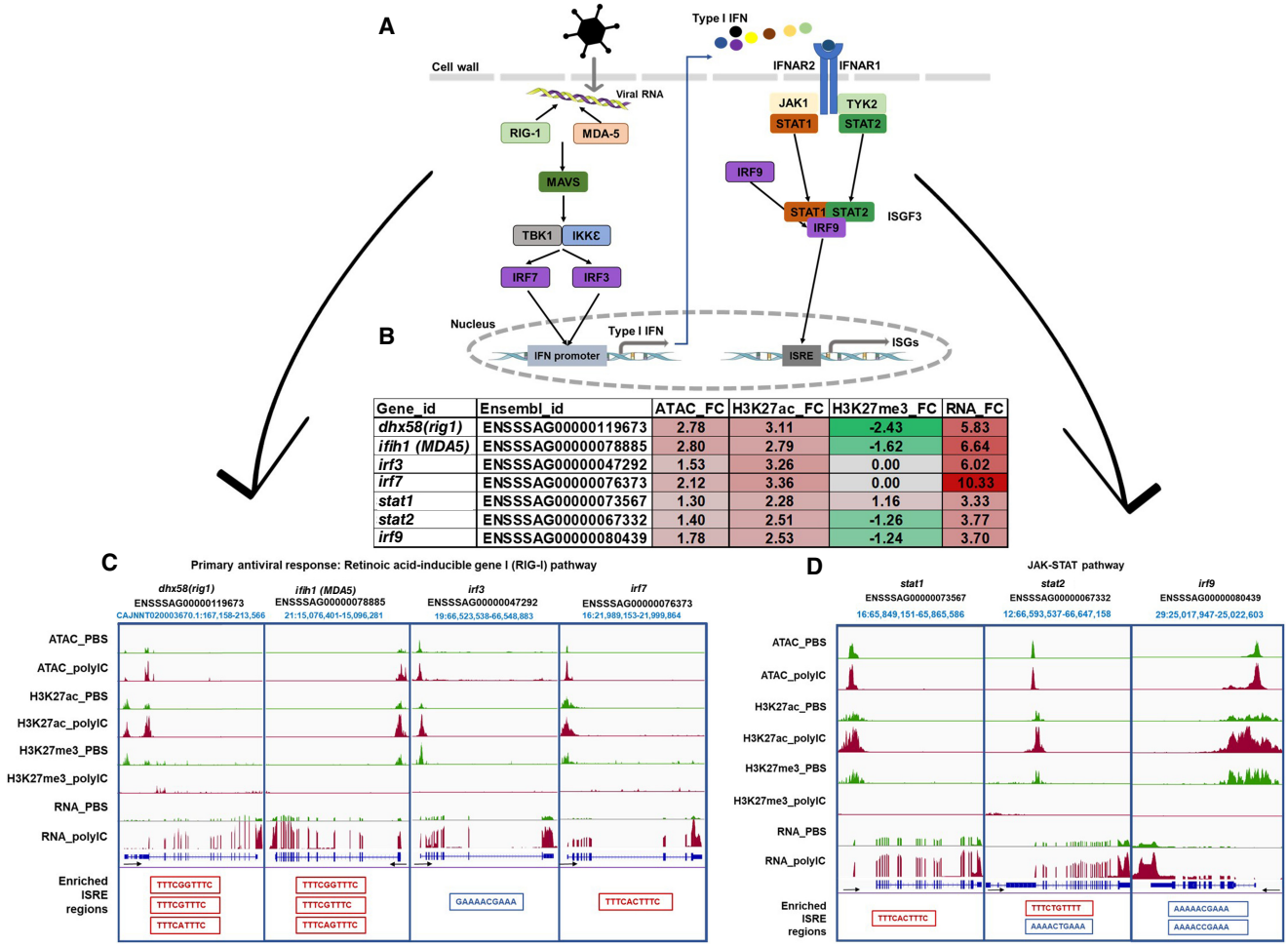
Our analysis revealed significant alterations in both the transcriptome and "regulome" in response to poly I:C stimulation. Notably, these changes were observed in a subset of conversed ISGs, which play an important role in antiviral defense in all vertebrates. ATAC-seq provided valuable insights into chromatin accessibility alterations during the antiviral response, revealing hundreds of regions exhibiting significant changes following poly I:C stimulation. The functional significance of these open

Downloaded from genome.cshlp.org on November 17, 2026 . Published by Cold Spring Harbor Laboratory Press



chromatin regions was supported by enrichment of Gene Ontology terms related to viral response for the nearby genes they presumably regulate. H3K27ac and H3K27me3 histone modifications are key players in gene regulation (Barski et al. 2007; Creyghton et al. 2010). Our study revealed a significant increase in H3K27ac activity in 1539 genomic regions, indicative of gene activation. Conversely, the upregulation of H3K27me3 in 795 regions suggests transcriptional suppression and the formation of repressive chromatin structures. Only 30 genomic regions exhibited concurrent changes in both H3K27ac and H3K27me3. Although these marks are typically considered mutually exclusive, their detection within the same genomic regions is likely to reflect cell-type heterogeneity, in which the same regulatory element is repressed (H3K27me3) in some cell populations while being active (H3K27ac) in others. This may indicate differential regulatory states across distinct cell subsets rather than a true bivalent chromatin state (Barral and Déjardin 2023). These regions may play critical roles in maintaining essential cellular processes or fine-tuning immune response regulation, potentially through mechanisms involving chromatin remodeling and transcription factor recruitment. Collectively, the integration of ATAC-seq and ChIP-seq data provides comprehensive insights into regulatory changes in Atlantic salmon in response to viral stimulation.

We find 3541 genes that show differential expression following poly I:C stimulation, which together are consistent with different layers of regulatory changes representing different functional groups of genes. The core set of 197 genes that are transcriptionally upregulated and also have significant increased open chromatin and increased presence of activating H3K27ac is enriched in ISGs conserved among vertebrates (Clark et al. 2023). Of interest there were also genes that showed chromatin remodeling, with no associated significant change in gene expression. These genes may represent a group of loci with distinct temporal regulation, potentially primed for expression either before or after the single time point analyzed in our study. For instance, genes that exhibited changes in chromatin accessibility and gene expression without accompanying H3K27ac modifications, suggest the involvement of distal enhancers or alternative chromatin dynamics such as topologically associating domains (TADs) influencing their regulation (Tena and Pereira 2021). The genes that are defined as having chromatin




| Gene_id | Ensembl_id | ATAC_FC | H3K27ac_FC | H3K27me3_FC | RNA_FC |
|---|---|---|---|---|---|
| *dhx58(rig1)* | ENSSSAG00000119673 | 2.78 | 3.11 | -2.43 | 5.83 |
| *ifih1 (MDA5)* | ENSSSAG00000078885 | 2.80 | 2.79 | -1.62 | 6.64 |
| *irf3* | ENSSSAG00000047292 | 1.53 | 3.26 | 0.00 | 6.02 |
| *irf7* | ENSSSAG00000076373 | 2.12 | 3.36 | 0.00 | 10.33 |
| *stat1* | ENSSSAG00000073567 | 1.30 | 2.28 | 1.16 | 3.33 |
| *stat2* | ENSSSAG00000067332 | 1.40 | 2.51 | -1.26 | 3.77 |
| *irf9* | ENSSSAG00000080439 | 1.78 | 2.53 | -1.24 | 3.70 |

**Figure 6.** Antiviral IFN-response processes. (*A*) A schematic view illustrating the type I IFN signaling pathway, encompassing both primary and secondary responses. (*B*) A table displaying the genes involved in the RIG-I and JAK-STAT pathways, along with their fold change values from the differential gene expression analysis. The color coding indicates upregulation (red), downregulation (green), and no response (gray). (*C*,*D*) IGV visualizations of the RIG-I and JAK-STAT pathway genes derived from the ATAC-seq, ChIP-seq, and RNA-seq data sets. The visualizations also include the enriched ISRE motifs associated with each gene. The direction of the gene transcription is indicated by the black arrow below the gene structure.

Downloaded from genome.cshlp.org on November 17, 2026 . Published by Cold Spring Harbor Laboratory Press



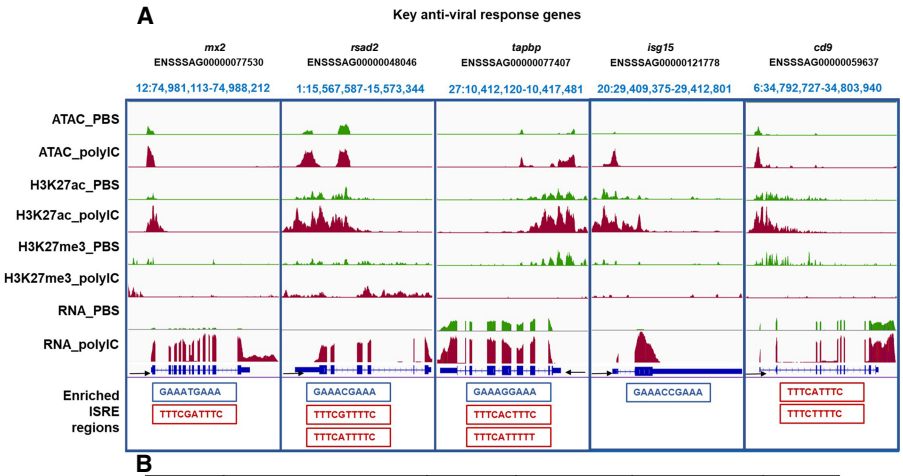
openness and increased expression have very clear IFN-associated functionality, which could reflect different activation modes of histone modification (H3K4me3 and H3K4me1), as in our study we examined a single activating histone mark (Murphy et al. 2025). The large number of genes that are transcriptionally upregulated but lack significant changes in chromatin accessibility and histone acetylation (H3K27ac) exhibit a very clear role in the IFN response. These genes likely represent early response genes that are already in an accessible chromatin state, allowing for rapid transcriptional activation upon stimulation (Bahrami and Diabløs 2016). Alternatively, these genes may be regulated post-transcriptionally following poly I:C stimulation, a mechanism often observed in innate immune responses, which could involve mRNA stability, translation efficiency, or degradation pathways (Carpenter et al. 2014).

Recent single-cell transcriptomic studies have highlighted the remarkable cellular heterogeneity of Atlantic salmon immune cells, particularly in the head kidney (Andresen et al. 2024) and in the liver (Taylor et al. 2022). This diversity likely underlies the observed largely disconnected regulation of H3K27ac and H3K27me3 marks in response to poly I:C, as different immune cell subpopulations likely exhibit distinct patterns of chromatin remodeling at the same loci. Although a detailed, locus-by-locus inspection was beyond the scope of this study, our findings are consistent with the idea that cellular heterogeneity shapes the chromatin and transcriptional responses to antiviral stimulation. Incorporating such single-cell insights in future studies will be valuable for resolving how specific cell types contribute to the epigenomic regulation of the IFN response in salmonid immunity.

ISREs are DNA sequence motifs responsible for the regulation of immune genes (Au et al. 1995), which serve as recognition sites for transcription factors integral to the IFN-response pathway (Ivashkiv and Donlin 2014). Our analysis identified a notable enrichment of TFBSs specific to IRF8, IRF9, STAT1, and STAT2 in response to poly I:C stimulation. These transcription factors are well documented to bind to ISREs (Au-Yeung et al. 2013; Platanitis et al. 2019), underlining the significance of transcription factor–mediated regulatory mechanisms governing the antiviral immune response in Atlantic salmon. IRF8 exhibited the highest level of enrichment in those genes that were identified across the RNA-seq, ATAC-seq, and H3K27ac data sets. These genes included key antiviral effectors, such as *TRIM21*-homolog, *MEFV*, and *PARP14*, which are involved in protein ubiquitination, immune modulation, and transcriptional activation of ISGs. IRF8, a transcription factor that binds to ISREs to regulate antiviral gene expression, is critical for immune responses across vertebrates. In humans and mice, IRF8 is crucial for the development and function of dendritic cells and macrophages, which are key players in antiviral defense and type I IFN production (Laricchia-Robbio et al. 2005; Hambleton et al. 2011). Studies on IRF8-deficient mice have demonstrated increased susceptibility to viral infections, linked to compromised dendritic cell populations and disrupted immune signaling pathways (Becker et al. 2012; Moorman et al. 2022). These findings, combined with the strong enrichment of IRF8 motifs in our data set, highlight its evolutionary conservation and central role in orchestrating the antiviral immune response in Atlantic salmon.

Moreover, these transcription factors are known regulators of immune response genes during viral infections (Ivashkiv and Donlin 2014). Our analysis demonstrates that ISRE-containing genomic regions undergo dynamic histone modifications during antiviral signaling, indicating their functional relevance in gene regulation. This study also expands upon previous research on ISREs in salmonids, focusing on gene families such as *mx*, *rsad2*, *stat1*, *stat2*, and *cd9*, which were previously examined primarily at the expression level (Collet 2004; Castro et al. 2008, 2010; Holland et al. 2008; Collins et al. 2014; Dehler et al. 2023). Earlier studies included in silico promoter analyses and reporter gene assays, but our integration of ATAC-seq and ChIP-seq data sets allows demarcation of genomic regions with putative functional involvement in the early antiviral response. However, further experimental validation, such as knockout or knock-in studies targeting the identified regulatory elements, will be essential to confirm the molecular mechanisms underlying these observations.

The enrichment of TFBSs associated with IRF3 and IRF7 underscores their important role in the antiviral response of Atlantic salmon. The enrichment of TFBSs for PRDM1, IRF6, JDP2, NR2E1, and BCL6 highlights the diverse regulatory landscape governing the immune response in Atlantic salmon following poly I:C stimulation. PRDM1 (also known as BLIMP-1) is known for regulating type I IFN and differentiation of B




B

| Gene_id | Ensembl_id | ATAC_FC | H3K27ac_FC | H3K27me3_FC | RNA_FC |
|---|---|---|---|---|---|
| *mx2* | ENSSSAG00000077530 | 6.91 | 4.56 | 1.77 | 23.84 |
| *rsad2* | ENSSSAG00000048046 | 2.56 | 2.62 | -2.05 | 86.03 |
| *tapbp* | ENSSSAG00000077407 | 2.40 | 2.38 | 0.00 | 2.89 |
| *isg15* | ENSSSAG00000121778 | 4.12 | 2.17 | 0.00 | 44.79 |
| *cd9* | ENSSSAG00000059637 | 2.21 | 2.17 | -1.46 | 3.36 |

**Figure 7.** Visualization of key antiviral response genes. (*A*) IGV visualizations of ATAC-seq, ChIP-seq, and RNA-seq data for the genes *mx2, rsad2, tapbp, isg15, and cd9*. The visualizations illustrate the chromatin accessibility, histone modification profiles, and gene expression patterns associated with each gene. Enriched ISRE motifs specific to each gene are identified, indicating their regulatory importance in driving the antiviral response. Arrows next to the transcripts indicate the direction of the sequence. (*B*) Table summarizing the gene expression data for *mx2, rsad2, tapbp, isg15, and cd9*. Red indicates upregulation, green indicates downregulation, and gray indicates no response. The table provides a concise overview of the transcriptional changes exhibited by these key antiviral response genes following stimulation with poly I:C.

Downloaded from genome.cshlp.org on November 17, 2026 . Published by Cold Spring Harbor Laboratory Press



cells into plasma cells (Lin et al. 1997), but it also orchestrates plasma cell differentiation by extinguishing the mature B cell gene expression program (Shaffer et al. 2002), whereas BCL6 is involved in B cell development in mammalian germinal centers (Tsai et al. 2019). IRF6 further contributes to antiviral responses (Liang et al. 2022). JDP2 has a core role in modulating inflammatory signaling pathways (Maruyama et al. 2012), and NR2E1 is involved in neural development and has a crucial role in regulating the proliferation, differentiation, and maintenance of neural progenitor cells in various regions of the brain (Islam and Zhang 2015). Despite our TFBS analysis relying on the JASPER database, primarily employing experimental data on mammalian transcription factors as the background, the enrichment of these TFBSs in response to poly I:C suggests their evolutionary conservation across vertebrate species, underscoring their relevance in understanding immune responses beyond Atlantic salmon.

Our analysis of enrichment in paralog-specific ISRE motifs unveiled distinctive ISRE sequences exclusive to specific paralogs. Consequences of four rounds of WGD (two in early vertebrates, one in the teleost ancestor, and one salmonid specific) can be detected in the Atlantic salmon genome, a phenomenon well documented in the literature (Lien et al. 2016). This process has given rise to multiple paralogous genes that have evolved distinct regulation (e.g., Gillard et al. 2021), as observed for many ISG families (Clark et al. 2023). We identified paralog-specific alterations in the chromatin accessibility of key ISGs, including genes such as *mx*, *rsad2*, *cd9*, *rigi*, *stat1*, *irf7*, and *irf9*. One outcome following gene duplication and frequent subsequent silencing of the particular paralog could relate to insertion of transposable elements into the regulatory regions of ISGs as was suggested for a decrease transcriptional activity across salmonid genomes in which ohnologs showing decreased expression had great abundance of transposable elements (Gillard et al. 2021). In line with this genomic complexity, immune gene families exhibit heterogeneous distribution patterns, with some, such as finTRIMs, in gene groups dispersed across the genome, whereas others, including MHC class I genes, form a few or a unique cluster on a specific location (Van der Aa et al. 2009; Lukacs et al. 2010). These findings underscore the importance of considering paralog-specific responses in investigations of the IFN response in salmonids and other species with a history of WGDs.

This study has demonstrated the activation of putative regulatory elements initiating the antiviral response in a teleost fish by integrating transcriptomics and regulomics. We identified a conserved set of ISGs showing increased mRNA expression following antiviral stimulation, which is likely a product of transcriptional changes induced by remodeling of chromatin state and histone modifications. We further discovered the importance of paralog-specific changes in key TFBSs, indicating that the regulatory control of key immune genes has been altered in the recent evolutionary history of salmonids. This work provides a new reference for functional analysis of immune response of Atlantic salmon/fish using transcriptomics and genomics and frames it in an evolutionary perspective.

## Methods

### Animal studies

Juvenile Atlantic salmon (~70 g) of commercial origin were maintained in 250 L freshwater tanks in the zoology building aquarium at the University of Aberdeen (School of Biological Sciences). Water temperature was maintained at 14°C, and fish were fed a commercial pellet diet. The water flow rate was ~1000 L/h, and the photoperiod was 12:12 light–dark. All procedures described complied with the Animal (Scientific Procedures) Act of 1986 under the UK Home Office license PFF8CC5BE and were approved by the ethics committee at the University of Aberdeen, Scotland, United Kingdom.

### Stimulation of fish with viral mimic

The poly I:C (Sigma-Aldrich P1530) was diluted to 5 mg/mL in PBS, aliquoted, and stored at − 20°C. Prior to being used for immune stimulation, poly I:C was heated for 15 min at 55°C and then allowed to cool at room temperature for 20 min. Fish were anaesthetized using 2-phenoxyethanol (2.5 mL in 10 L water/ 0.0025% v/v) and given an intraperitoneal injection of either PBS (1×, 0.1 mL; $n = 6$, controls) or poly I:C (500 µg in 0.1 mL, per fish; $n = 6$). Twenty-four hours after stimulation, fish were euthanized by overexposure to 2-phenoxyethanol followed by destruction of the brain using a scalpel. Head kidney tissue was sampled, which was chosen for this study as the primary hematopoietic tissue in teleosts, rich in different leucocyte populations. For RNA-seq, samples were stored in RNAlater (Sigma-Aldrich) for 24 h at 4°C followed by long-term storage at −80°C. For ATAC-seq and ChIP-seq, fresh head kidney tissue was placed in L15 media (Gibco) containing 2% FBS (Labtech) and 0.02% EDTA (Sigma-Aldrich) and placed on ice until processing. For each fish ($n = 6$ per PBS and poly I:C injected groups) one RNA-seq, one ATAC-seq, and two ChIP-seq libraries (H3K27ac and H3K27me3 histone marks; see later section) were constructed from the same head kidney sample to facilitate data integration (Supplemental Fig. 1).

### ATAC-seq library preparation

ATAC-seq library preparation was adapted from the method of Buenrostro et al. (2015). Head kidney tissue (~20 mg) was placed into a 50 mL tube (tube 1) containing 20 mL extraction media (L15, 2% FBS, and 0.02% EDTA at pH 8). The tissue was gently passed through a 100 µm nylon mesh (Starlab) and placed in a new 50 mL tube using a sterile pipette and spatula. Extraction medium was continually applied to prevent cells from drying out and assist with their transit through the mesh. This step disrupted the tissue, and cells were dissociated in the media. The final suspension of cells was made up to 20 mL in extraction media. An aliquot of 10 µL of these cells was mixed with trypan blue (Sigma-Aldrich) at a 1:5 ratio and counted using a hemocytometer. An aliquot of 75,000 cells for each sample was transferred in a 1.5 mL loBind Eppendorf tube for ATAC-seq library preparation, and the remaining cells were retained for ChIP-seq library generation as described in a later section.

Head kidney nuclei were isolated by pelleting the cells by centrifugation (500*g*, 5 min, 4°C). The supernatant was discarded carefully by aspiration to avoid cell loss. The cells were washed by resuspending and then gentle pipetting in 1 mL PBS containing protease inhibitor cocktail (PIC; Sigma-Aldrich). The cells were pelleted again (5 min at 500*g* at 4°C); the supernatant was removed, to which 50 µL of cold ATAC-resuspension buffer L (ATAC-RSB-L) containing 0.1% Tween-20, 0.1% NP-40, and 0.01% digitonin (Promega) was added to the cell pellet, and suspended by gently pipetting up and down three times. The ATAC-RSB cold buffer was made up of 1 M Tris (pH 7.4, Sigma-Aldrich), 5 M NaCl (Sigma-Aldrich), 1 M $MgCl_2$ (Sigma-Aldrich), and $dH_2O$. Cells were incubated on ice for 3 min in cold ATAC-RSB-L to lyse the cells and release intact nuclei. Immediately after 3 min, 1 mL of ATAC-RSB-W (ATAC-RSB-W contains ATAC-RSB and 10% Tween-

Downloaded from genome.cshlp.org on November 17, 2026 . Published by Cold Spring Harbor Laboratory Press



20) with 0.1% Tween-20 was added to the lysed cells. The tube was inverted three times and then centrifuged for 10 min at 800*g* at 4°C to pellet the nuclei before the supernatant was aspirated carefully to avoid losing the pellet.

The remaining ATAC-seq library preparation steps, such as transposase reaction, clean-up using MinElute PCR purification, library amplification, and library clean-up, were performed according to the method of Buenrostro et al. (2015).

### ChIP-seq library preparation

ChIP-seq libraries were generated using the ChIPmentation kit for histones (Diagenode C010110009). After tissue disruption and dissociation of cells in the extraction media, as described above for ATAC-seq, $2 \times 10^6$ cells were transferred into a 1.5 mL tube and pelleted for 10 min at 800*g* at 4°C before the supernatant was carefully removed. Next, 1 mL of formaldehyde solution 1% (Sigma-Aldrich) was added, and the pellet was then resuspended by pipetting up and down and incubated under constant rotation at room temperature for 5 min to cross-link the DNA and proteins. The reaction was quenched by the addition of 125 µL of 1 M glycine (0.125 M final) and incubated for 10 min at room temperature under constant rotation. The cross-linked cells were centrifuged for 5 min at 1000*g* at 4°C, and the supernatant was removed. Next, cells were resuspended in 1 mL of PBS with PIC by pipetting and centrifuged for 5 min at 1000*g* at 4°C before the supernatant was removed, and the cell pellet was stored at −80°C.

Sonication using a Bioruptor pico device (Diagenode) was optimized at 20 cycles and 30 sec on/30 sec off to disrupt the cells and shear the DNA. The sonicated chromatin was processed using the MinElute PCR purification kit (Qiagen). Twenty microliters of sonicated chromatin was added to 180 µL elution buffer along with 2 µL of RNase A (100 mg/mL) and incubated for 10 min at 37°C. Five microliters of Proteinase K (20 mg/mL) was added before further incubation for 1 h at 68°C under constant rotation. DNA purification was performed using the MinElute PCR purification kit (Qiagen). DNA was then quantified using NanoDrop (One/One microvolume UV-Vis spectrophotometer, Thermo Fisher Scientific) and assessed by Tapestation (4200, Agilent Technologies) with a high-sensitivity DNA kit to determine DNA fragment size. A fragment size range of 100–700 bp was achieved for all downstream ChIP-seq library preparations. The remaining steps followed Diagenode's instructions for the ChIPmentation kit. The two antibodies used were H3K27ac (Diagenode C15410196) and H3K27me3 (Diagenode C15410195). For the control input, an IgG antibody (Diagenode code C15400001-15) was used in each series of ChIP reactions. The input samples consisted of a pooled mixture of all six samples within the respective group.

### Sequencing and data analysis

For ATAC-seq and ChIP-seq, paired-end 150 bp libraries were sequenced using an Illumina NovaSeq 6000 platform by Novogene, aiming to generate 40 million reads per sample (see Data access). For RNA-seq, we used the differentially expressed data published by Clark et al. (2023), which was from matched samples available from the the European Nucleotide Archive (ENA; https://www.ebi.ac.uk/ena/browser/home) under accession number PRJEB50076.

For ATAC-seq and ChIP-seq, the processing of raw reads, mapping of reads, peak calling, and quantification was performed using the nextflow pipelines, nf-core/atacseq (v2.0) and nf-core/chipseq (v2.0). Raw reads were trimmed using Trim Galore! (v0.6.10; https://github.com/FelixKrueger/TrimGalore) and adapters removed. All reads were mapped to the current Atlantic salmon reference genome (GCA_905237065.2) downloaded from the Ensembl genome browser release Ssal_v3.1 (https://www.ensembl.org/Salmo_salar/Info/Index). Mapping was carried out using BWA (v0.7.17) (Li and Durbin 2009), and consensus peak calling for ATAC-seq and ChIP-seq were performed using MACS2 (Zhang et al. 2008). Peaks were annotated using HOMER (v4.9.1) (Heinz et al. 2010), and consensus peaks were quantified using featureCounts (Liao et al. 2014). Input controls were included in the peak-calling process to normalize background signal and enhance the specificity of peak identification. The sequence-specific mapping and individually selected genes were visualized using the Integrative Genomics Viewer (IGV) tools (Thorvaldsdottir et al. 2013).

The quantified ATAC-Seq and ChIP-Seq peaks were imported into R v4.2.2 (R Core Team 2022), and differential peak analysis was performed using DESeq2 (Love et al. 2014). Significantly different peaks among groups were identified using the Wald test in DESeq2 following false-discovery rate (FDR) correction using the Benjamini–Hochberg approach, with adjusted $P$-value < 0.05 and up or down fold change > 2.

### Gene set enrichment analysis

To identify biological processes associated with differentially accessible or modified chromatin regions, we performed region-centric enrichment analysis using the R package rGREAT (Gu and Hübschmann 2023), which interfaces with the Genomic Regions Enrichment of Annotations Tool. This approach allows functional enrichment analysis directly from genomic coordinates without requiring prior gene assignment, preserving the spatial resolution of the ATAC-seq and ChIP-seq data sets.

Differentially accessible ATAC-seq regions and differentially abundant H3K27ac regions were supplied to rGREAT as query sets in BED format and imported into R as GRanges objects. For each analysis, the background set was defined as the full set of consensuses ATAC-seq or H3K27ac peaks, respectively, to control for assay-specific genomic coverage and avoid biases from using the whole genome as background. Enrichment was tested against Gene Ontology biological process (GO:BP) terms using the Atlantic salmon genome annotation (GTF file) and the Ensembl *S. salar* data set (ssalar_gene_ensembl) provided by rGREAT. GO terms with an adjusted $P$-value < 0.05 were considered significantly enriched. In addition, gene expression–centric enrichment analysis was performed using the Database of Annotation, Visualization, and Integrated Discovery (DAVID; v2023q4) (Huang et al. 2009) on the list of differentially expressed genes identified by RNA-seq. Human orthologs of the Atlantic salmon genes were identified following the approach of Clark et al. (2023). In cases in which multiple paralogs were expressed for a single gene, the paralog with the highest expression was selected. The background gene set for DAVID was the human gene repertoire. GO terms with fold enrichment >2 and FDR-adjusted $P$ < 0.05 were considered enriched.

### Chromatin-state discovery

ChromHMM (v1.24) was used to identify genome-wide chromatin states using the integrated ATAC-seq, H3K27ac, and H3K27me3 ChIP-seq data sets. ChromHMM uses a multivariate hidden Markov model that considers the spatial and combinatorial arrangements of various chromatin marks to learn and describe these states (Ernst and Kellis 2012). First, the aligned reads for each sample were converted into a binarized format using the BinarizeBam function with the following command: java

Downloaded from genome.cshlp.org on November 17, 2026 . Published by Cold Spring Harbor Laboratory Press



-mx4000M -jar ChromHMM.jar BinarizeBam CHROMSIZES/Ssal_v3.1.txt inputbam samplefile.txt binarize outputdir. We then used the LearnModel function to develop models of chromatin states based on these binary files, automatically generating chromatin-state segmentation across the genome. To start model learning and have automatic enrichments computed after the model is learned, the LearnModel command was computed: java -mx4000M -jar ChromHMM.jar LearnModel -p 64 inputdir outputdir 5 Ssal_v3.1. Chromatin states were annotated by ChromHMM using the five-state model based on enrichment of ATAC-seq and H3K27ac signals (active) or H3K27me3 signal (repressive). Promoter regions were defined as the chromatin segments annotated by ChromHMM as promoter-like states and overlapping the annotated TSSs from the *S. salar* genome annotation. TSS coordinates were derived directly from the reference GTF and correspond to the 5′ end of each transcript.

### TFBS analysis

For the TFBS prediction and analysis, we used GimmeMotifs (Bruse and van Heeringen 2018) with the JASPAR2022 vertebrate core database (Castro-Mondragon et al. 2022); the database comprises curated, nonredundant binding motifs derived from experimental evidence. Motif enrichment was assessed using active regulatory regions from ChromHMM state 5 (active enhancers and promoters) in poly I:C–stimulated and control PBS samples. To reduce false positives, background-matched genomic regions were used, and a *Z*-score threshold of more than two was applied to retain only significantly enriched motifs associated with antiviral responses.

## Data access

The raw sequence data generated in this study have been submitted to the European Nucleotide Archive (ENA) (https://www.ebi.ac.uk/ena/browser/home) under accession numbers PRJEB50076 (RNA-seq), PRJEB50077 (ATAC-seq), and PRJEB56698 (ChIP-seq). Metadata from this study can be found at the AQUA-FAANG Data Portal (https://data.faang.org/projects/AQUA-FAANG).

## Competing interest statement

The authors declare no competing interests.

## Acknowledgments

This work was funded by the European Union's Horizon 2020 research and innovation program under grant agreement no. 817923 (AQUAFAANG) and Biotechnology and Biological Sciences Research Council project BB/W008564/1.

*Author contributions*: S.N. was responsible for conceptualization, methodology, investigation, data curation, writing the original draft, and reviewing and editing. T.C. was responsible for conceptualization, methodology, investigation, data curation, writing the original draft, and reviewing and editing. D.J.M. was responsible for conceptualization, methodology, investigation, data curation, supervision, funding acquisition, writing the original draft, and reviewing and editing. D.B. was responsible for methodology and reviewing and editing. B.C. was responsible for conceptualization, methodology, investigation, and reviewing and editing. P.D. was responsible for methodology, investigation, data curation, and reviewing and editing. P.B. was responsible for conceptualization, methodology, investigation, data curation, supervision, funding acquisition, writing the original draft, and reviewing and editing. S.A.M.M. was responsible for conceptualization, methodology, investigation, data curation, supervision, funding acquisition, writing the original draft, and reviewing and editing.

## References

An LL, Gong XY, Dan C, Sun HY, Guo WH, Luan HY, Wu MY, Yu JC, Zhang YB. 2025. Family evolution and functional divergence of bony fish-specific Gig1 homologs. *Water Biol Secur* **4:** 100382. doi:10.1016/j.watbs.2025.100382

Andresen AM, Taylor RS, Grimholt U, Daniels RR, Sun J, Dobie R, Henderson NC, Martin SA, Macqueen DJ, Fosse JH. 2024. Mapping the cellular landscape of Atlantic salmon head kidney by single cell and single nucleus transcriptomics. *Fish Shellfish Immunol* **146:** 109357. doi:10.1016/j.fsi.2024.109357

Au WC, Moore PA, Lowther W, Juang YT, Pitha PM. 1995. Identification of a member of the interferon regulatory factor family that binds to the interferon-stimulated response element and activates expression of interferon-induced genes. *Proc Natl Acad Sci* **92:** 11657–11661. doi:10.1073/pnas.92.25.11657

Au-Yeung N, Mandhana R, Horvath CM. 2013. Transcriptional regulation by STAT1 and STAT2 in the interferon JAK-STAT pathway. *JAKSTAT* **2:** e23931. doi:10.4161/jkst.23931

Bahrami S, Drabløs F. 2016. Gene regulation in the immediate-early response process. *Adv Biol Regul* **62:** 37–49. doi:10.1016/j.jbior.2016.05.001

Barral A, Déjardin J. 2023. The chromatin signatures of enhancers and their dynamic regulation. *Nucleus* **14:** 2160551. doi:10.1080/19491034.2022.2160551

Barski A, Cuddapah S, Cui K, Roh T-Y, Schones DE, Wang Z, Wei G, Chepelev I, Zhao K. 2007. High-resolution profiling of histone methylations in the human genome. *Cell* **129:** 823–837. doi:10.1016/j.cell.2007.05.009

Becker AM, Michael DG, Satpathy AT, Sciammas R, Singh H, Bhattacharya D. 2012. IRF-8 extinguishes neutrophil production and promotes dendritic cell lineage commitment in both myeloid and lymphoid mouse progenitors. *Blood* **119:** 2003–2012. doi:10.1182/blood-2011-06-364976

Bernstein BE, Mikkelsen TS, Xie X, Kamal M, Huebert DJ, Cuff J, Fry B, Meissner A, Wernig M, Plath K, et al. 2006. A bivalent chromatin structure marks key developmental genes in embryonic stem cells. *Cell* **125:** 315–326. doi:10.1016/j.cell.2006.02.041

Biacchesi S, LeBerre M, Lamoureux A, Louise Y, Lauret E, Boudinot P, Brémont M. 2009. Mitochondrial antiviral signaling protein plays a major role in induction of the fish innate immune response against RNA and DNA viruses. *J Virol* **83:** 7815–7827. doi:10.1128/jvi.00404-09

Bosselut R. 2016. Pleiotropic functions of H3K27Me3 demethylases in immune cell differentiation. *Trends Immunol* **37:** 102–113. doi:10.1016/j.it.2015.12.004

Boudinot P, Salhi S, Blanco M, Benmansour A. 2001. Viral haemorrhagic septicaemia virus induces vig-2, a new interferon-responsive gene in rainbow trout. *Fish Shellfish Immunol* **11:** 383–397. doi:10.1006/fsim.2000.0326

Briolat V, Jouneau L, Carvalho R, Palha N, Langevin C, Herbomel P, Schwartz O, Spaink HP, Levraud J-P, Boudinot P. 2014. Contrasted innate responses to two viruses in zebrafish: insights into the ancestral repertoire of vertebrate IFN-stimulated genes. *J Immunol* **192:** 4328–4341. doi:10.4049/jimmunol.1302611

Bruse N, van Heeringen SJ. 2018. GimmeMotifs: an analysis framework for transcription factor motif analysis. bioRxiv doi:10.1101/474403

Buenrostro JD, Wu B, Chang HY, Greenleaf WJ. 2015. ATAC-seq: a method for assaying chromatin accessibility genome-wide. *Curr Protoc Mol Biol* **109:** 21.29.1–21.29.9. doi:10.1002/0471142727.mb2129s109

Caprara G, Prosperini E, Piccolo V, Sigismondo G, Melacarne A, Cuomo A, Boothby M, Rescigno M, Bonaldi T, Natoli G. 2018. PARP14 controls the nuclear accumulation of a subset of type I IFN–inducible proteins. *J Immunol* **200:** 2439–2454. doi:10.4049/jimmunol.1701117

Carpenter S, Ricci E, Mercier B, Moore MJ, Fitzgerald KA. 2014. Post-transcriptional regulation of gene expression in innate immunity. *Nat Rev Immunol* **14:** 361–376. doi:10.1038/nri3682

Castro R, Martin SAM, Bird S, Lamas J, Secombes CJ. 2008. Characterisation of γ-interferon responsive promoters in fish. *Mol Immunol* **45:** 3454–3462. doi:10.1016/j.molimm.2008.03.015

Castro R, Martin SAM, Zou J, Secombes CJ. 2010. Establishment of an IFN-γ specific reporter cell line in fish. *Fish Shellfish Immunol* **28:** 312–319. doi:10.1016/j.fsi.2009.11.010

Castro-Mondragon JA, Riudavets-Puig R, Rauluseviciute I, Berhanu Lemma R, Turchi L, Blanc-Mathieu R, Lucas J, Boddie P, Khan A, Manosalva

Downloaded from genome.cshlp.org on November 17, 2026 . Published by Cold Spring Harbor Laboratory Press



Pérez N, et al. 2022. JASPAR 2022: the 9th release of the open-access database of transcription factor binding profiles. *Nucleic Acids Res* **50:** D165–D173. doi:10.1093/nar/gkab1113
Clark T, Naseer S, Gundappa MK, Laurent A, Perquis A, Collet B, Macqueen DJ, Martin SAM, Boudinot P. 2023. Conserved and divergent arms of the antiviral response in the duplicated genomes of salmonid fishes. *Genomics* **115:** 110663. doi:10.1016/j.ygeno.2023.110663
Collet B. 2004. An Mx1 promoter–reporter system to study interferon pathways in rainbow trout. *Dev Comp Immunol* **28:** 793–801. doi:10.1016/j.dci.2003.12.005
Collet B, Secombes CJ. 2001. The rainbow trout (*Oncorhynchus mykiss*) *Mx1* promoter. *Eur J Biochem* **268:** 1577–1584. doi:10.1046/j.1432-1327.2001.02021.x
Collet B, Ganne G, Bird S, Collins CM. 2009. Isolation and expression profile of a gene encoding for the signal transducer and activator of transcription STAT2 in Atlantic salmon (*Salmo salar*). *Dev Comp Immunol* **33:** 821–829. doi:10.1016/j.dci.2009.01.007
Collins C, Ganne G, Collet B. 2014. Isolation and activity of the promoters for STAT1 and 2 in Atlantic salmon *Salmo salar*. *Fish Shellfish Immunol* **40:** 644–647. doi:10.1016/j.fsi.2014.07.025
Cooper L, Xu H, Polmear J, Kealy L, Szeto C, Pang ES, Gupta M, Kirn A, Taylor JJ, Jackson KJ, et al. 2024. Type I interferons induce an epigenetically distinct memory B cell subset in chronic viral infection. *Immunity* **57:** 1037–1055.e6. doi:10.1016/j.immuni.2024.03.016
Creyghton MP, Cheng AW, Welstead GG, Kooistra T, Carey BW, Steine EJ, Hanna J, Lodato MA, Frampton GM, Sharp PA, et al. 2010. Histone H3K27ac separates active from poised enhancers and predicts developmental state. *Proc Natl Acad Sci* **107:** 21931–21936. doi:10.1073/pnas.1016071107
Dehler CE, Lester K, Della Pelle G, Jouneau L, Houel A, Collins C, Dovgan T, Machat R, Zou J, Boudinot P, et al. 2019. Viral resistance and IFN signaling in STAT2 knockout fish cells. *J Immunol* **203:** 465–475. doi:10.4049/jimmunol.1801376
Dehler CE, Boudinot P, Collet B, Martin SAM. 2023. Phylogeny and expression of tetraspanin CD9 paralogues in rainbow trout (*Oncorhynchus mykiss*). *Dev Comp Immunol* **146:** 104735. doi:10.1016/j.dci.2023.104735
Ernst J, Kellis M. 2012. ChromHMM: automating chromatin-state discovery and characterization. *Nat Methods* **9:** 215–216. doi:10.1038/nmeth.1906
Ernst J, Kellis M. 2017. Chromatin-state discovery and genome annotation with ChromHMM. *Nat Protoc* **12:** 2478–2492. doi:10.1038/nprot.2017.124
Gan Z, Chen SN, Huang B, Zou J, Nie P. 2020. Fish type I and type II interferons: composition, receptor usage, production and function. *Rev Aquac* **12:** 773–804. doi:10.1111/raq.12349
Gillard GB, Grønvold L, Røsæg LL, Holen MM, Monsen Ø, Koop BF, Rondeau EB, Gundappa MK, Mendoza J, Macqueen DJ, et al. 2021. Comparative regulomics supports pervasive selection on gene dosage following whole genome duplication. *Genome Biol* **22:** 103. doi:10.1186/s13059-021-02323-0
Gu Z, Hübschmann D. 2023. *rGREAT*: an R/Bioconductor package for functional enrichment on genomic regions. *Bioinformatics* **39:** btac745. doi:10.1093/bioinformatics/btac745
Haller O, Stertz S, Kochs G. 2007. The Mx GTPase family of interferon-induced antiviral proteins. *Microbes Infect* **9:** 1636–1643. doi:10.1016/j.micinf.2007.09.010
Hambleton S, Salem S, Bustamante J, Bigley V, Boisson-Dupuis S, Azevedo J, Fortin A, Haniffa M, Ceron-Gutierrez L, Bacon CM, et al. 2011. *IRF8* mutations and human dendritic-cell immunodeficiency. *N Engl J Med* **365:** 127–138. doi:10.1056/NEJMoa1100066
Harvey TN, Gillard GB, Røsæg LL, Grammes F, Monsen Ø, Vik JO, Hvidsten TR, Sandve SR. 2024. The genome regulatory landscape of Atlantic salmon liver through smoltification. *PLoS One* **19:** e0302388. doi:10.1371/journal.pone.0302388
Heinz S, Benner C, Spann N, Bertolino E, Lin YC, Laslo P, Cheng JX, Murre C, Singh H, Glass CK. 2010. Simple combinations of lineage-determining transcription factors prime *cis*-regulatory elements required for macrophage and B cell identities. *Mol Cell* **38:** 576–589. doi:10.1016/j.molcel.2010.05.004
Holland JW, Bird S, Williamson B, Woudstra C, Mustafa A, Wang T, Zou J, Blaney SC, Collet B, Secombes CJ. 2008. Molecular characterization of IRF3 and IRF7 in rainbow trout, *Oncorhynchus mykiss*: functional analysis and transcriptional modulation. *Mol Immunol* **46:** 269–285. doi:10.1016/j.molimm.2008.08.265
Huang DW, Sherman BT, Lempicki RA. 2009. Systematic and integrative analysis of large gene lists using DAVID bioinformatics resources. *Nat Protoc* **4:** 44–57. doi:10.1038/nprot.2008.211
Islam MM, Zhang C-L. 2015. TLX: a master regulator for neural stem cell maintenance and neurogenesis. *Biochim Biophys Acta* **1849:** 210–216. doi:10.1016/j.bbagrm.2014.06.001
Ivashkiv LB, Donlin LT. 2014. Regulation of type I interferon responses. *Nat Rev Immunol* **14:** 36–49. doi:10.1038/nri3581
Kan RL, Chen J, Sallam T. 2022. Crosstalk between epitranscriptomic and epigenetic mechanisms in gene regulation. *Trends Genet* **38:** 182–193. doi:10.1016/j.tig.2021.06.014
Koepke L, Gack MU, Sparrer KM. 2021. The antiviral activities of TRIM proteins. *Curr Opin Microbiol* **59:** 50–57. doi:10.1016/j.mib.2020.07.005
Langevin C, Boudinot P, Collet B. 2019. IFN signaling in inflammation and viral infections: new insights from fish models. *Viruses* **11:** 302. doi:10.3390/v11030302
Laricchia-Robbio L, Tamura T, Karpova T, Sprague BL, McNally JG, Ozato K. 2005. Partner-regulated interaction of IFN regulatory factor 8 with chromatin visualized in live macrophages. *Proc Natl Acad Sci* **102:** 14368–14373. doi:10.1073/pnas.0504014102
Levraud J-P, Jouneau L, Briolat V, Laghi V, Boudinot P. 2019. IFN-stimulated genes in zebrafish and humans define an ancient arsenal of antiviral immunity. *J Immunol* **203:** 3361–3373. doi:10.4049/jimmunol.1900804
Li H, Durbin R. 2009. Fast and accurate short read alignment with Burrows–Wheeler transform. *Bioinformatics* **25:** 1754–1760. doi:10.1093/bioinformatics/btp324
Li J, Rodriguez JP, Niu F, Pu M, Wang J, Hung LW, Shao Q, Zhu Y, Ding W, Liu Y, et al. 2016. Structural basis for DNA recognition by STAT6. *Proc Natl Acad Sci* **113:** 13015–13020. doi:10.1073/pnas.1611228113
Liang Y, Liu R, Zhang J, Chen Y, Shan S, Zhu Y, Yang G, Li H. 2022. Negative regulation of interferon regulatory factor 6 (IRF6) in interferon and NF-κB signalling pathways of common carp (Cyprinus carpio L.). *BMC Vet Res* **18:** 433. doi:10.1186/s12917-022-03538-4
Liao Y, Smyth GK, Shi W. 2014. featureCounts: an efficient general purpose program for assigning sequence reads to genomic features. *Bioinformatics* **30:** 923–930. doi:10.1093/bioinformatics/btt656
Lien S, Koop BF, Sandve SR, Miller JR, Kent MP, Nome T, Hvidsten TR, Leong JS, Minkley DR, Zimin A, et al. 2016. The Atlantic salmon genome provides insights into rediploidization. *Nature* **533:** 200–205. doi:10.1038/nature17164
Lin Y, Wong K, Calame K. 1997. Repression of c-*myc* transcription by Blimp-1, an inducer of terminal B cell differentiation. *Science* **276:** 596–599. doi:10.1126/science.276.5312.596
Liu Y-J. 2005. IPC: professional type 1 interferon-producing cells and plasmacytoid dendritic cell precursors. *Annu Rev Immunol* **23:** 275–306. doi:10.1146/annurev.immunol.23.021704.115633
Love MI, Huber W, Anders S. 2014. Moderated estimation of fold change and dispersion for RNA-seq data with DESeq2. *Genome Biol* **15:** 550. doi:10.1186/s13059-014-0550-8
Lukacs MF, Harstad H, Bakke HG, Beetz-Sargent M, McKinnel L, Lubieniecki KP, Koop BF, Grimholt U. 2010. Comprehensive analysis of MHC class I genes from the U-, S-, and Z-lineages in Atlantic salmon. *BMC Genomics* **11:** 154. doi:10.1186/1471-2164-11-154
Mancino A, Termanini A, Barozzi I, Ghisletti S, Ostuni R, Prosperini E, Ozato K, Natoli G. 2015. A dual *cis*-regulatory code links IRF8 to constitutive and inducible gene expression in macrophages. *Genes Dev* **29:** 394–408. doi:10.1101/gad.257592.114
Macqueen DJ, Johnston IA. 2014. A well-constrained estimate for the timing of the salmonid whole genome duplication reveals major decoupling from species diversification. *Proc Biol Sci* **281:** 20132881. doi:10.1098/rspb.2013.2881
Martin SAM, Taggart JB, Seear P, Bron JE, Talbot R, Teale AJ, Sweeney GE, Høyheim B, Houlihan DF, Tocher DR, et al. 2007. Interferon type I and type II responses in an Atlantic salmon (*Salmo salar*) SHK-1 cell line by the salmon TRAITS/SGP microarray. *Physiol Genomics* **32:** 33–44. doi:10.1152/physiolgenomics.00064.2007
Maruyama K, Fukasaka M, Vandenbon A, Saitoh T, Kawasaki T, Kondo T, Yokoyama KK, Kidoya H, Takakura N, Standley D, et al. 2012. The transcription factor Jdp2 controls bone homeostasis and antibacterial immunity by regulating osteoclast and neutrophil differentiation. *Immunity* **37:** 1024–1036. doi:10.1016/j.immuni.2012.08.022
Matsumoto M, Funami K, Tanabe M, Oshiumi H, Shingai M, Seto Y, Yamamoto A, Seya T. 2003. Subcellular localization of toll-like receptor 3 in human dendritic cells. *J Immunol* **171:** 3154–3162. doi:10.4049/jimmunol.171.6.3154
Moorman HR, Reategui Y, Poschel DB, Liu K. 2022. IRF8: mechanism of action and health implications. *Cells* **11:** 2630. doi:10.3390/cells11172630
Mostafavi S, Yoshida H, Moodley D, LeBoité H, Rothamel K, Raj T, Ye CJ, Chevrier N, Zhang S-Y, Feng T, et al. 2016. Parsing the interferon transcriptional network and its disease associations. *Cell* **164:** 564–578. doi:10.1016/j.cell.2015.12.032
Murphy AE, Askarova A, Lenhard B, Skene NG, Marzi SJ. 2025. Predicting gene expression from histone marks using chromatin deep learning models depends on histone mark function, regulatory distance and cellular states. *Nucleic Acids Res* **53:** gkae1212. doi:10.1093/nar/gkae1212

Downloaded from genome.cshlp.org on November 17, 2026 . Published by Cold Spring Harbor Laboratory Press



Platanias LC. 2005. Mechanisms of type-I- and type-II-interferon-mediated signalling. *Nat Rev Immunol* **5:** 375–386. doi:10.1038/nri1604

Platanitis E, Demiroz D, Schneller A, Fischer K, Capelle C, Hartl M, Gossenreiter T, Müller M, Novatchkova M, Decker T. 2019. A molecular switch from STAT2-IRF9 to ISGF3 underlies interferon-induced gene transcription. *Nat Commun* **10:** 2921. doi:10.1038/s41467-019-10970-y

R Core Team. 2022. *R: a language and environment for statistical computing*. R Foundation for Statistical Computing, Vienna. https://www.R-project.org/.

Rehwinkel J, Gack MU. 2020. RIG-I-like receptors: their regulation and roles in RNA sensing. *Nat Rev Immunol* **20:** 537–551. doi:10.1038/s41577-020-0288-3

Robertson FM, Gundappa MK, Grammes F, Hvidsten TR, Redmond AK, Lien S, Martin SAM, Holland PWH, Sandve SR, Macqueen DJ. 2017. Lineage-specific rediploidization is a mechanism to explain time-lags between genome duplication and evolutionary diversification. *Genome Biol* **18:** 111. doi:10.1186/s13059-017-1241-z

Schoggins JW. 2019. Interferon-stimulated genes: What do they all do? *Annu Rev Virol* **6:** 567–584. doi:10.1146/annurev-virology-092818-015756

Shaffer AL, Lin KI, Kuo TC, Yu X, Hurt EM, Rosenwald A, Giltnane JM, Yang L, Zhao H, Calame K, et al. 2002. Blimp-1 orchestrates plasma cell differentiation by extinguishing the mature B cell gene expression program. *Immunity* **17:** 51–62. doi:10.1016/s1074-7613(02)00335-7

Skjesol A, Hansen T, Shi C-Y, Thim HL, Jørgensen JB. 2010. Structural and functional studies of STAT1 from Atlantic salmon (*Salmo salar*). *BMC Immunol* **11:** 17. doi:10.1186/1471-2172-11-17

Tamura T, Kurotaki D, Koizumi S. 2015. Regulation of myelopoiesis by the transcription factor IRF8. *Int J Hematol* **101:** 342–351. doi:10.1007/s12185-015-1761-9

Tan Q, Wang J, Hao Y, Yang S, Cao B, Pan W, Cao M. 2025. Elf1 deficiency impairs macrophage development in zebrafish model organism. *Int J Mol Sci* **26:** 2537. doi:10.3390/ijms26062537

Taylor RS, Ruiz Daniels R, Dobie R, Naseer S, Clark TC, Henderson NC, Boudinot P, Martin SA, Macqueen DJ. 2022. Single cell transcriptomics of Atlantic salmon (*Salmo salar* L.) liver reveals cellular heterogeneity and immunological responses to challenge by *Aeromonas salmonicida*. *Front Immunol* **13:** 984799. doi:10.3389/fimmu.2022.984799

Tena JJ, Santos-Pereira JM. 2021. Topologically associating domains and regulatory landscapes in development, evolution and disease. *Front Cell Dev Biol* **9:** 702787. doi:10.3389/fcell.2021.702787

Thompson MR, Kaminski JJ, Kurt-Jones EA, Fitzgerald KA. 2011. Pattern recognition receptors and the innate immune response to viral infection. *Viruses* **3:** 920–940. doi:10.3390/v3060920

Thorvaldsdottir H, Robinson JT, Mesirov JP. 2013. Integrative Genomics Viewer (IGV): high-performance genomics data visualization and exploration. *Brief Bioinformatics* **14:** 178–192. doi:10.1093/bib/bbs017

Tsai D-Y, Hung K-H, Chang C-W, Lin K-I. 2019. Regulatory mechanisms of B cell responses and the implication in B cell-related diseases. *J Biomed Sci* **26:** 64. doi:10.1186/s12929-019-0558-1

van Der Aa LM, Levraud JP, Yahmi M, Lauret E, Briolat V, Herbomel P, Benmansour A, Boudinot P. 2009. A large new subset of TRIM genes highly diversified by duplication and positive selection in teleost fish. *BMC Biol* **7:** 7. doi:10.1186/1741-7007-7-7

Wang Z, Zang C, Rosenfeld JA, Schones DE, Barski A, Cuddapah S, Cui K, Roh T-Y, Peng W, Zhang MQ, et al. 2008. Combinatorial patterns of histone acetylations and methylations in the human genome. *Nat Genet* **40:** 897–903. doi:10.1038/ng.154

Wang W, Xu L, Su J, Peppelenbosch MP, Pan Q. 2017. Transcriptional regulation of antiviral interferon-stimulated genes. *Trends Microbiol* **25:** 573–584. doi:10.1016/j.tim.2017.01.001

Zhang Y, Liu T, Meyer CA, Eeckhoute J, Johnson DS, Bernstein BE, Nusbaum C, Myers RM, Brown M, Li W, et al. 2008. Model-based Analysis of ChIP-Seq (MACS). *Genome Biol* **9:** R137. doi:10.1186/gb-2008-9-9-r137

Zou J, Secombes CJ. 2011. Teleost fish interferons and their role in immunity. *Dev Comp Immuno* **35:** 1376–1387. doi:10.1016/j.dci.2011.07.001

*Received February 18, 2025; accepted in revised form October 9, 2025.*